Equatorial Spread F – Observations

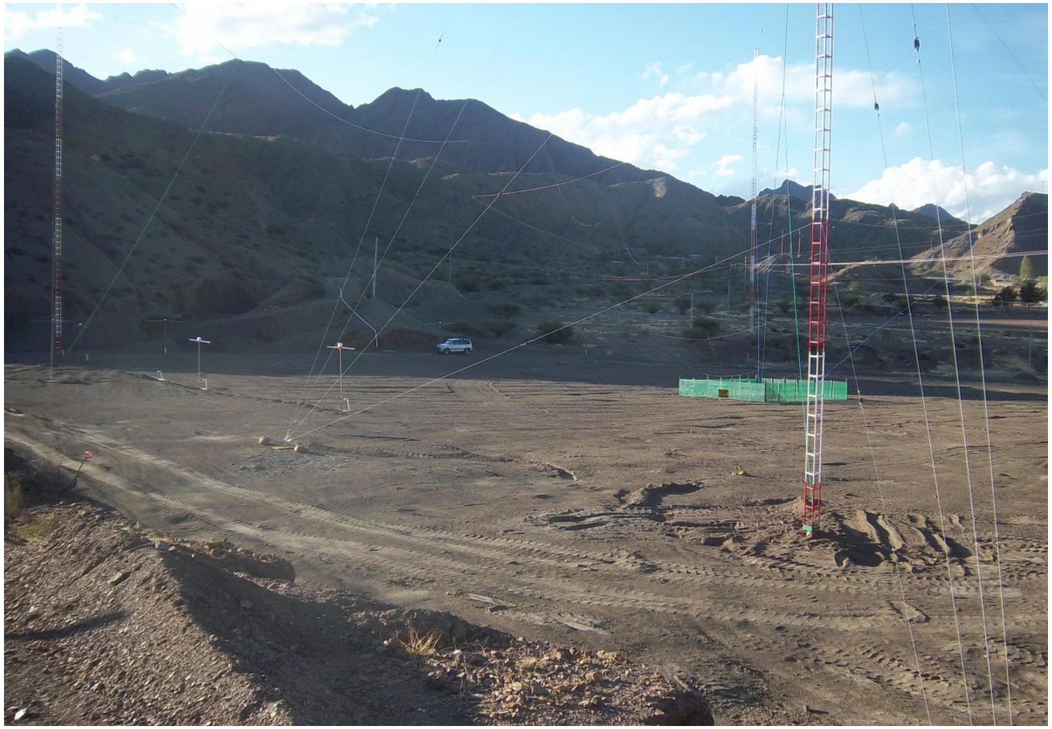

Cesar E. Valladares
Boston College
cesar.valladares@bc.edu

Outline

Two types of plasma irregularities at low latitudes: (1) Plasma bubbles (Radar plumes, TEC depletions, biteouts) and (2) Bottom-Side Sinusoids (BSS)

Different theories of Equatorial spread F. Gravity waves, Collisional Kelvin-Helmholtz instability, Wind-driven gradient drift and Large-scale wave structures (LSWS).

Statistical studies, global and regional.

Conclusions.

Bubbles

AE-E Plasma Bubbles

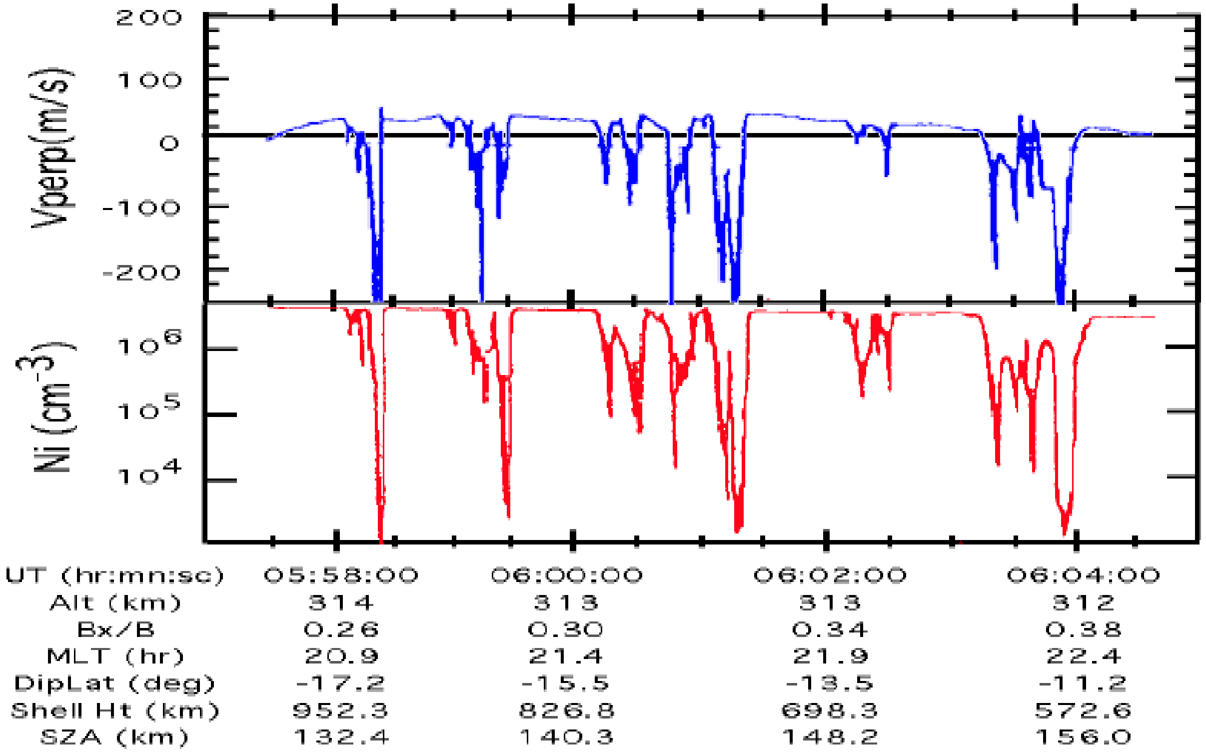

Vertical drifts

Number Density

Upward ion velocity in some bubbles increase approximately with δN reaching a limit much larger than the value predicted by R-T instability. These values may result from a Seed of the plasma bubbles.

Hanson and Bamgboye, JGR, 8997, 1984

Radar Plume, TEC depletion, and Scintillations September 06, 2002

A westward tilted plume reached 1650 km at 2100 LT. This altitude maps to the F region at 11° geographic North.

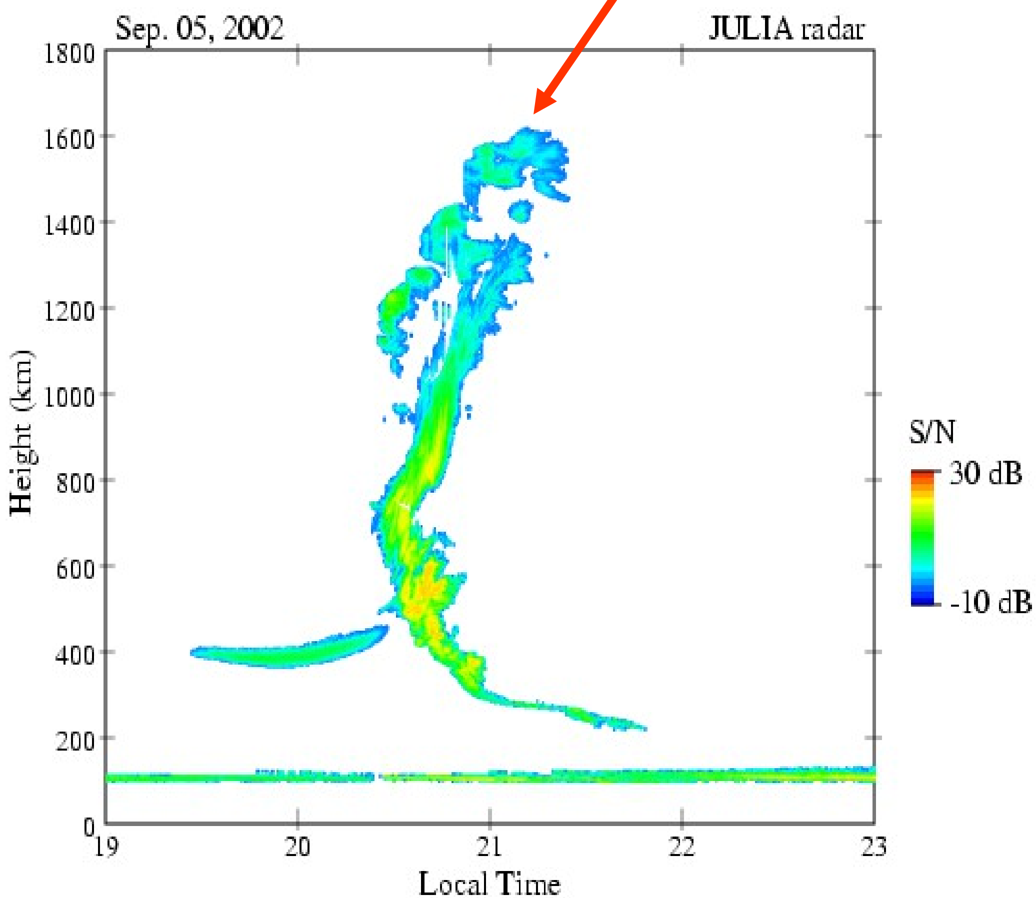

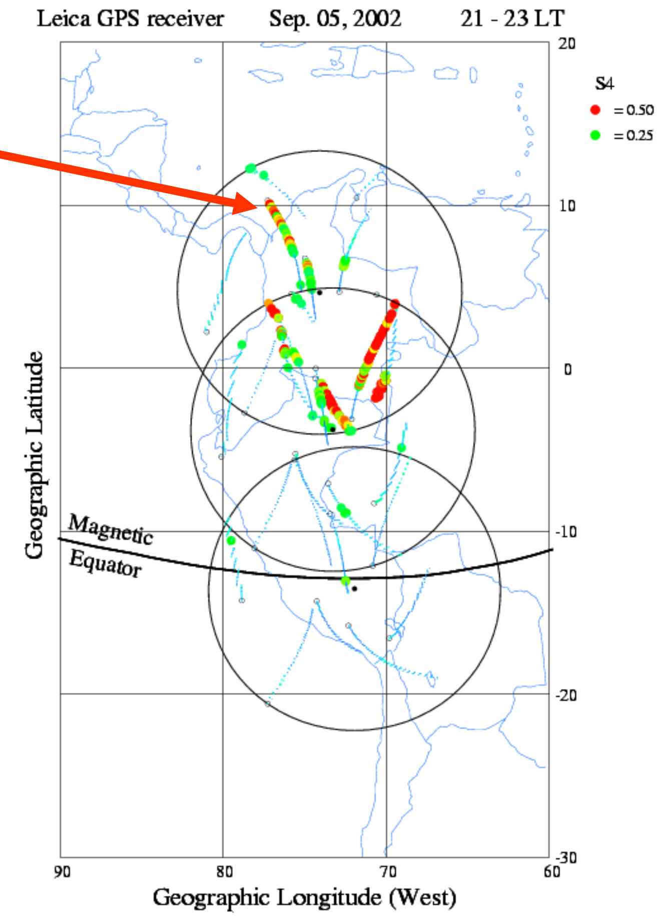

TEC and GPS scintillations

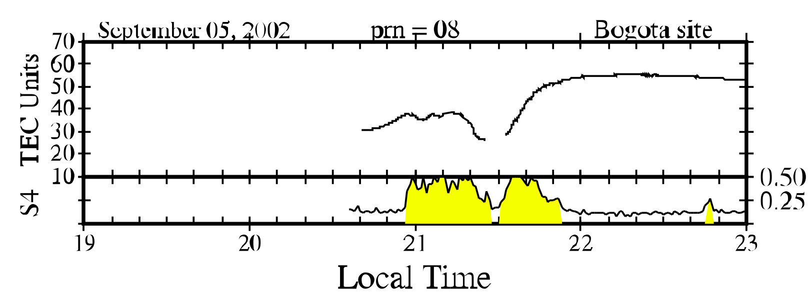

Plasma instabilities observed at Jicamarca Peru, on October 22, 1996

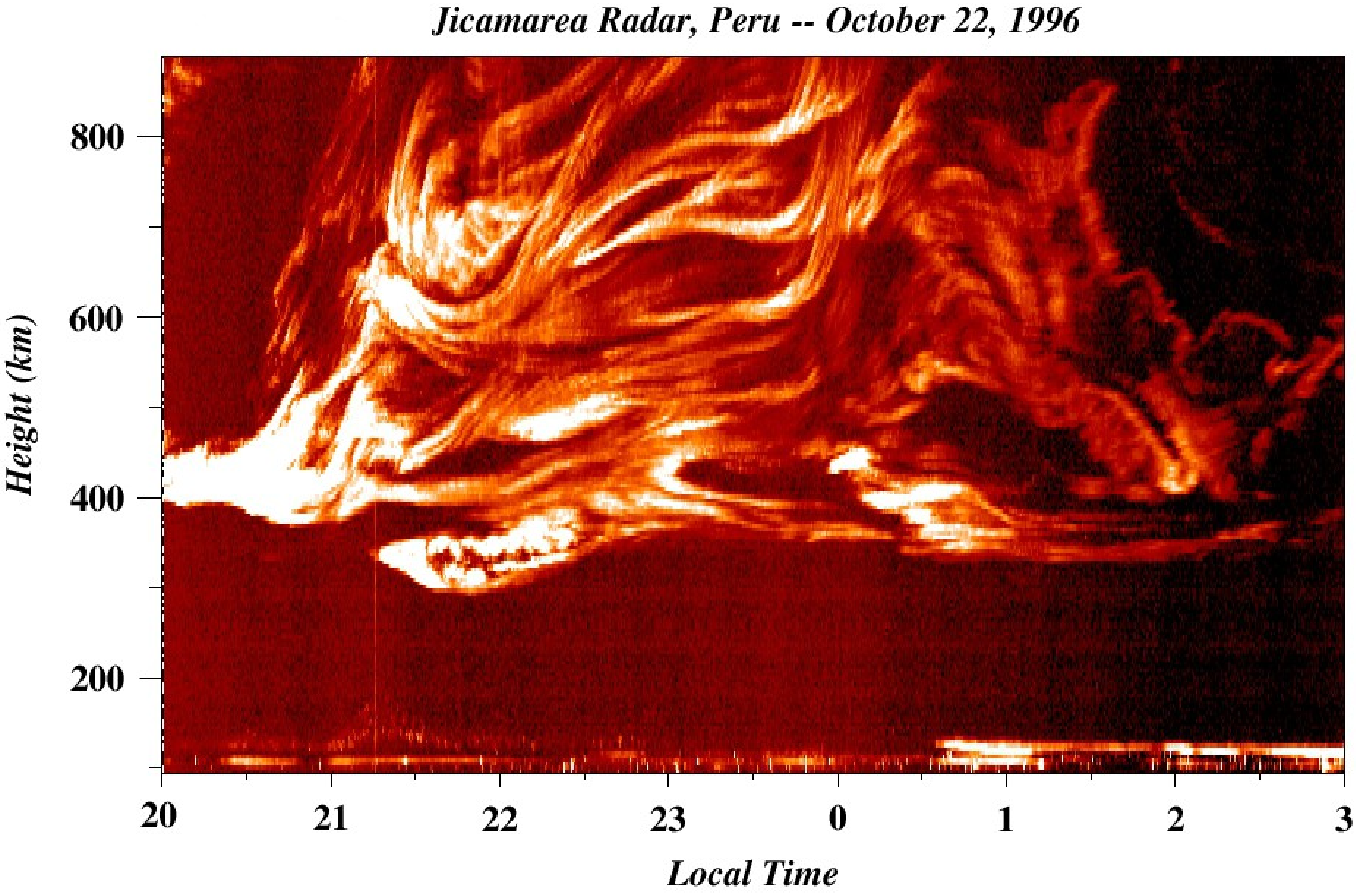

Depletions and Scintillation Recorded by the South American Chain of Stations

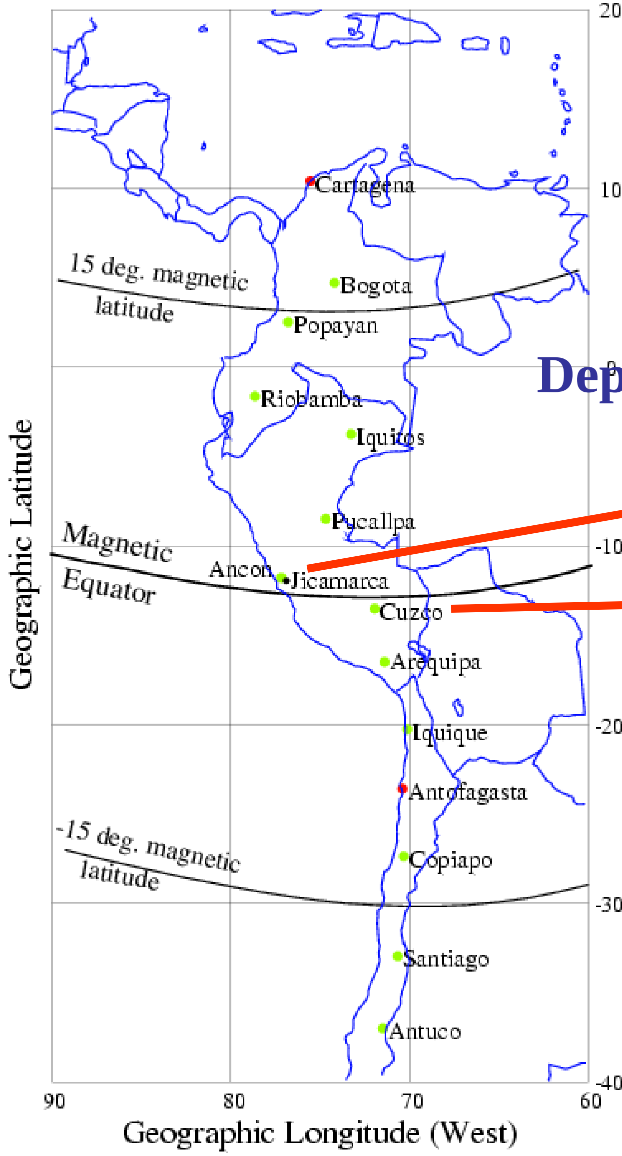

Depletion traveled at 140m/s

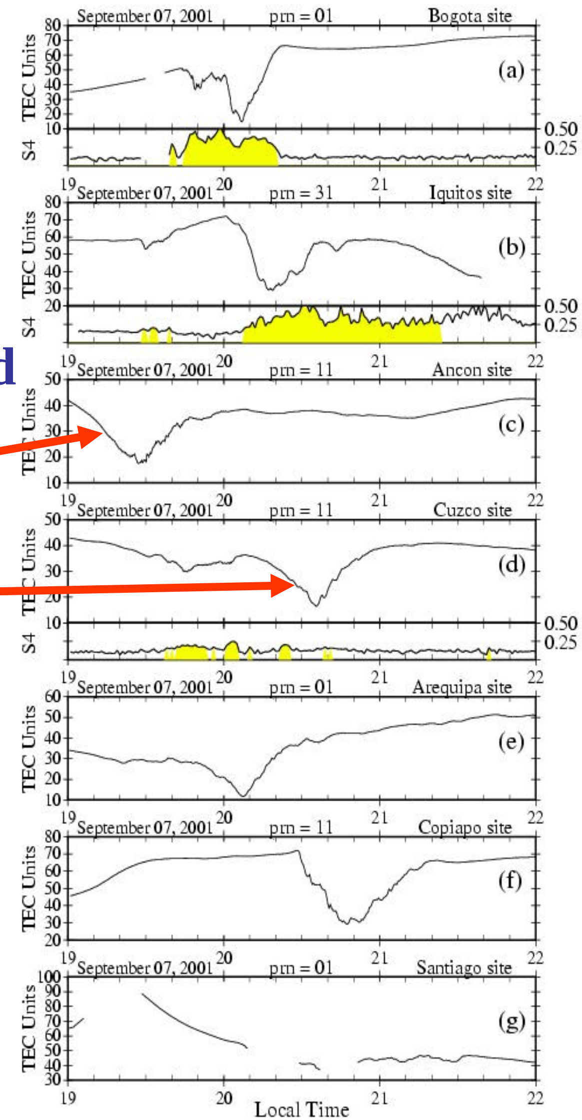

Radar plume associated with TEC depletions Feb 07, 2002

Due to the plume's westward tilt the TEC depletion is seen first at Iquitos (8°N) and then at Bogota (16°N).

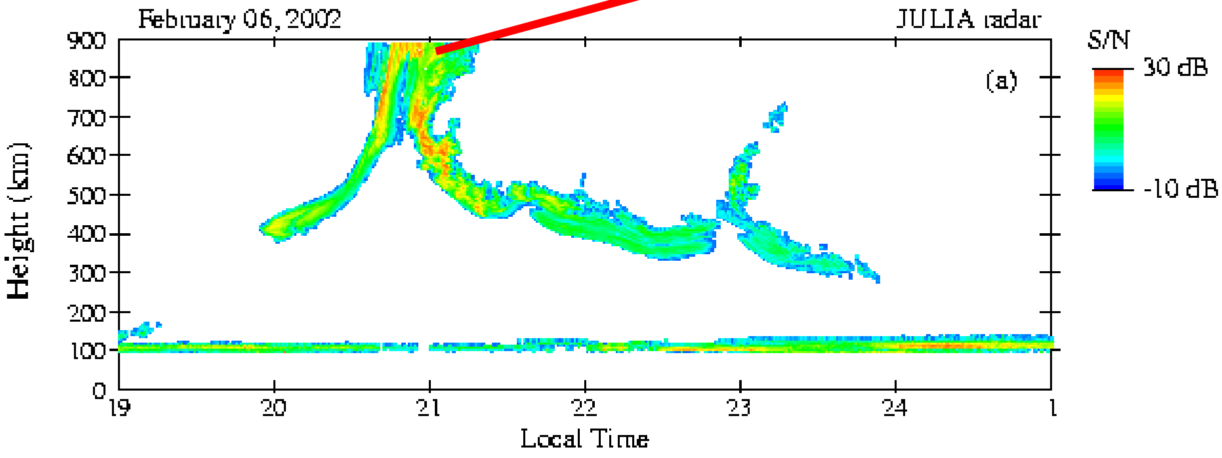

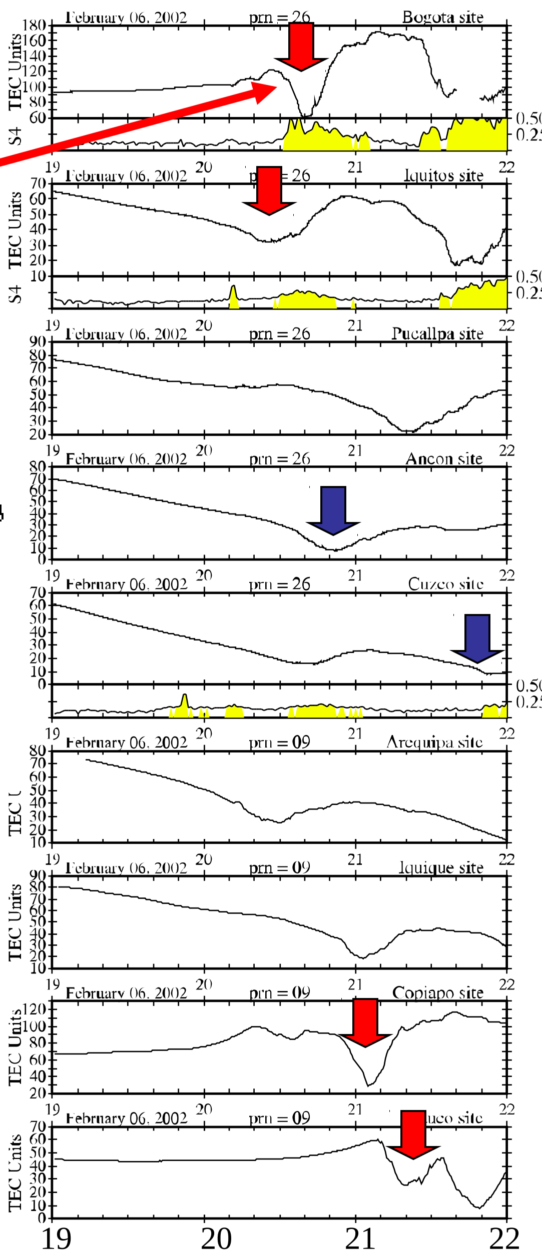

Near the magnetic equator the TEC depletions are only 20 TECU (blue arrows). Near the crests they are about 50 TECU (red arrows).

TEC, UHF Scintillations, and Ionograms
Feb 07, 2002

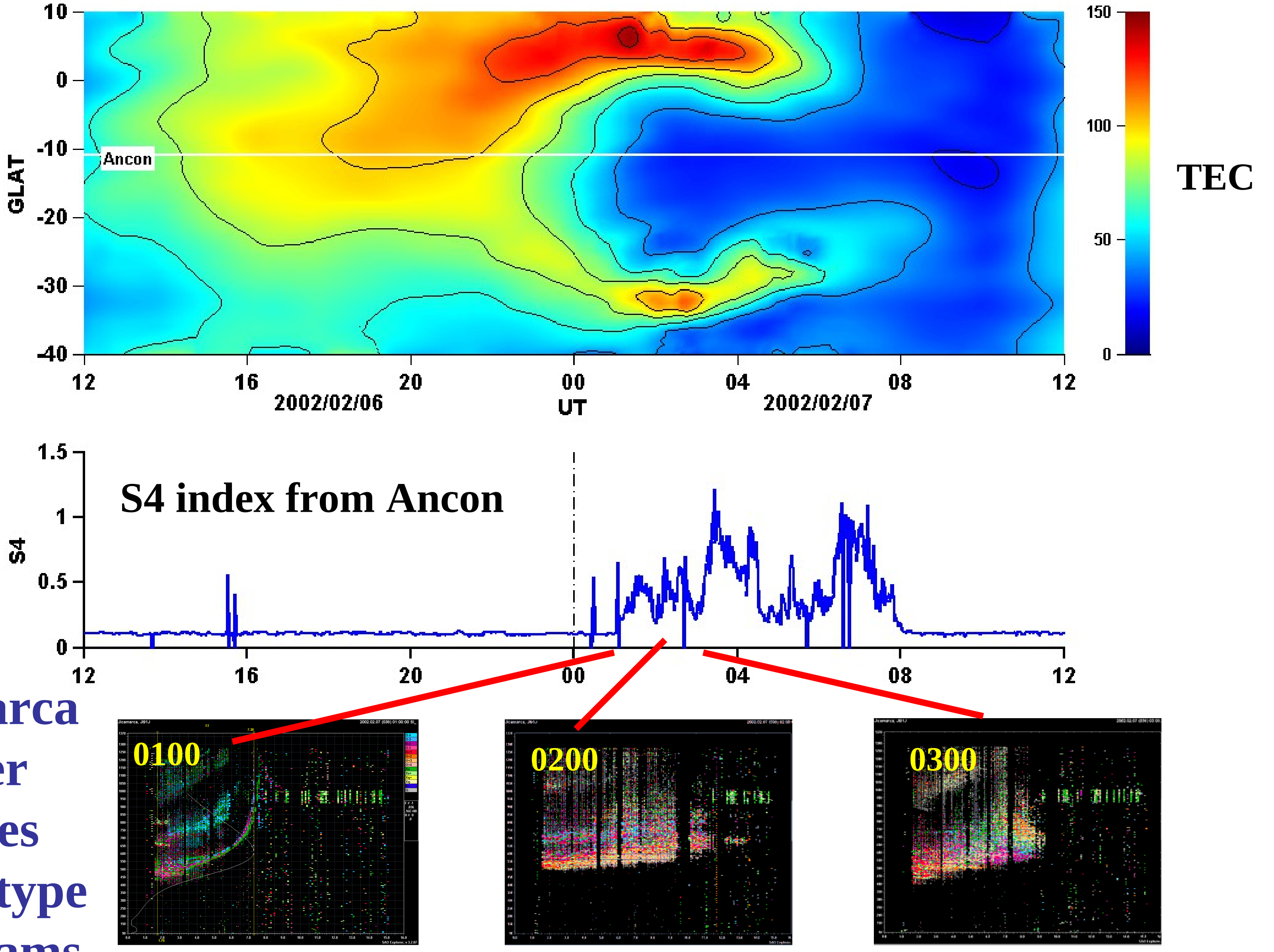

Jicamarca sounder observes range-type ionograms

Airglow depletions using 777.4 nm emissions

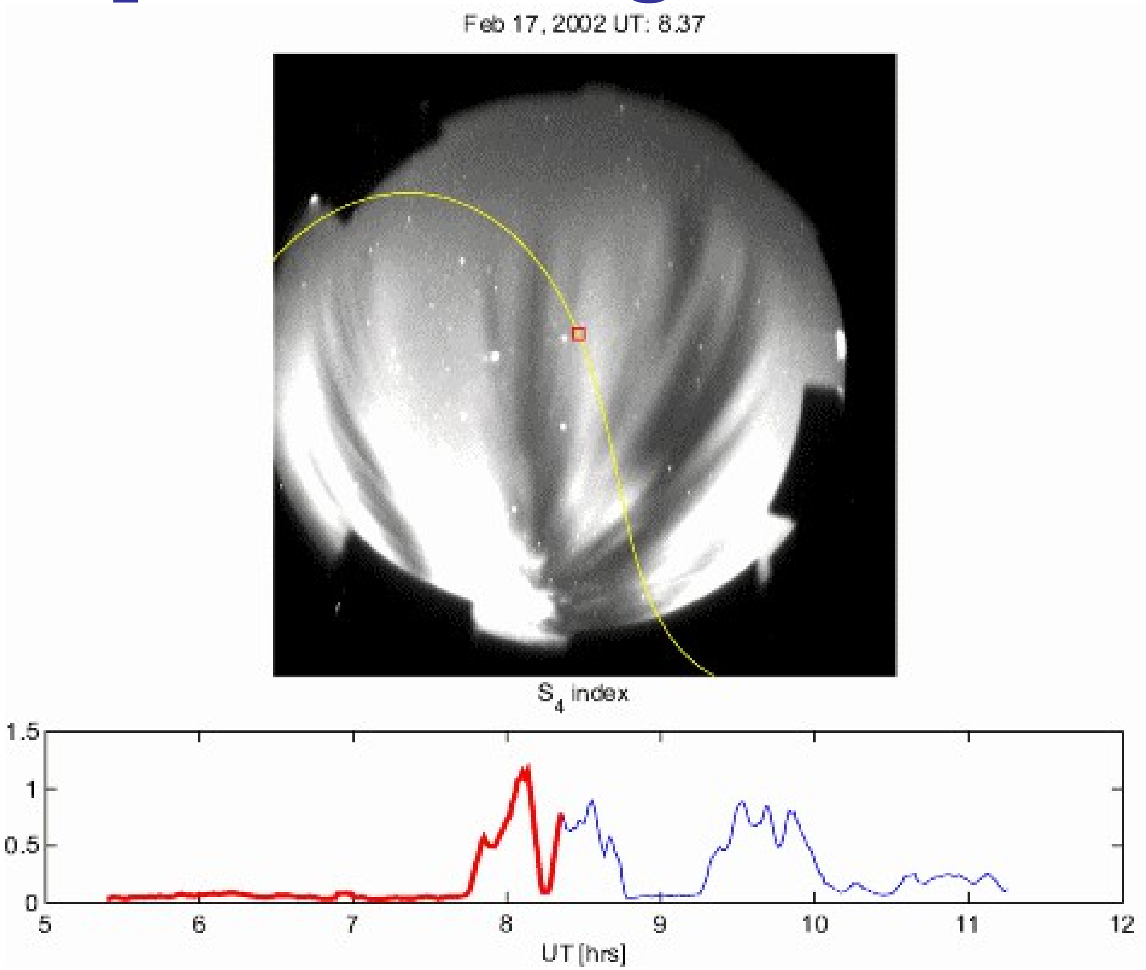

Haleakala all-sky camera (ASC) image and GPS scintillations. Severe scintillations, as shown in the lower panel by the S4 index from the GPS data, correlate to depleted regions of electron density (upper panel).

Makela et al., GRL, 2004

Plasma Bubbles Observed by ROCSAT

- **Pacific Depletions most often appear as bubble groups about 500 km wide in a background that is quite uniform.**

- **Africa depletions appear as bubble groups in excess of 1000 km wide in a background that has a large-scale depression.**

Pacific:

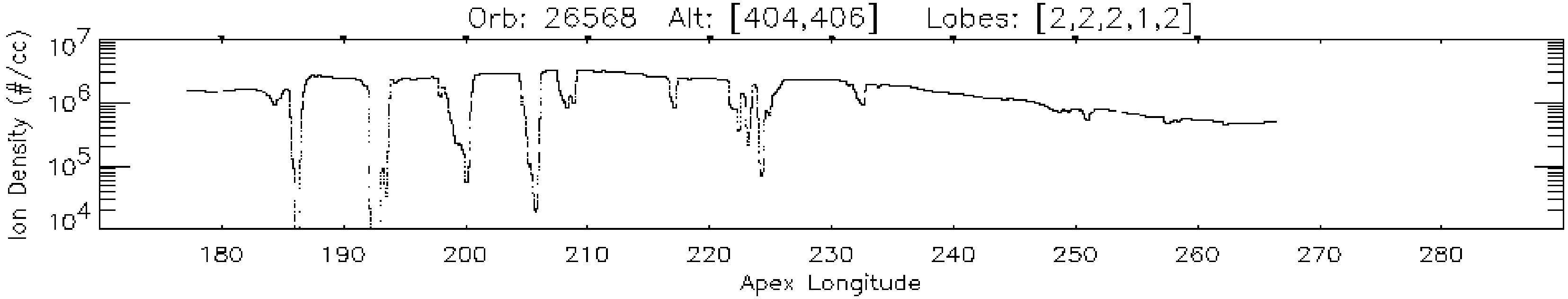

Africa:

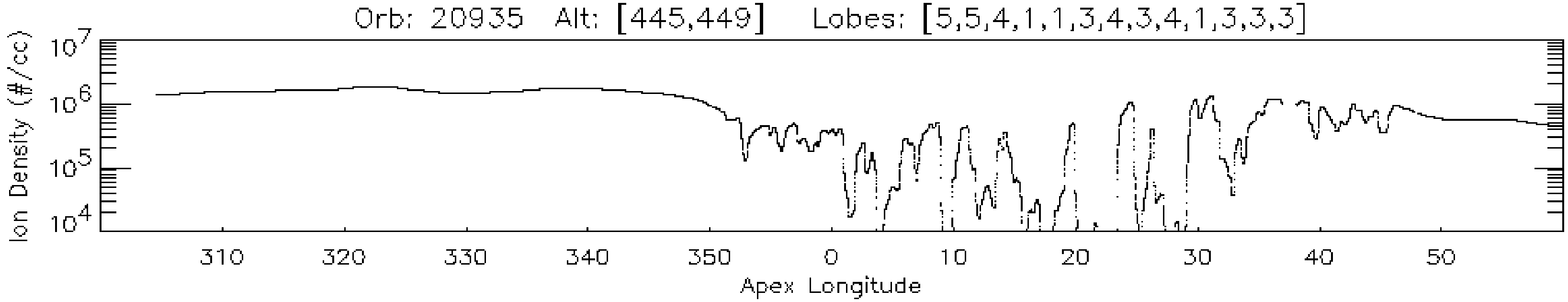

Hei, et al., seasonal and longitudinal variation of large-scale topside equatorial plasma depletions JGR, 2005.

The Rayleigh-Taylor Instability

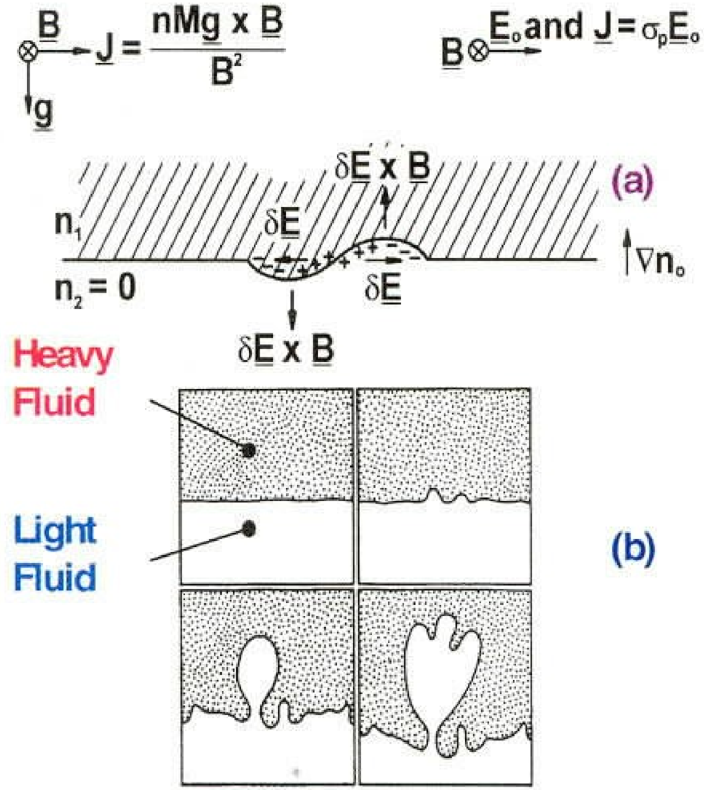

R-T Growth Rate

$$\gamma = \frac{\Sigma_P^F}{\Sigma_P^E + \Sigma_P^F}\left(V_p + U_n^P + \frac{g_L}{\nu_{in}^{eff}}\right)\frac{1}{L_n} - R_T$$

(a) Schematic diagram of the plasma analog of the hydrodynamic R-T instability in the equatorial geometry. (b) Sequential sketches from photos of the hydrodynamic R-T instability. A lighter fluid initially supports a heavy fluid.

Seeds, why we need seeds?

The calculated RTI growth rate for the evening ionosphere generally has an e-folding time of 15 minutes or greater. This is too slow for the observed rapid development of plasma plumes after sunset.

Atmospheric gravity waves can modulate the atmosphere through wind and electric field spatial variations that act as triggers of plasma bubbles [*Huang and Kelley*, 1996].

Seeds influence occurrence and properties of topside plasma structures. They may explain why the bubbles are highly depleted and densely packed in Africa instead of less depleted and widely spaced clusters in the Pacific sector [*Hei et al.*, 2005].

***Hysell and Kudeki* [2004] proposed a collisional Kelvin-Helmholtz instability that can quickly generate plasma irregularities that can then seed the RT instability for the non-linear development of plasma plumes.**

Satellite Measurements of Gravity Wave-induced Plasma Perturbations (Earle, et al., 2008)

Correlated Plasma and Neutral Densities below 300 km altitude.

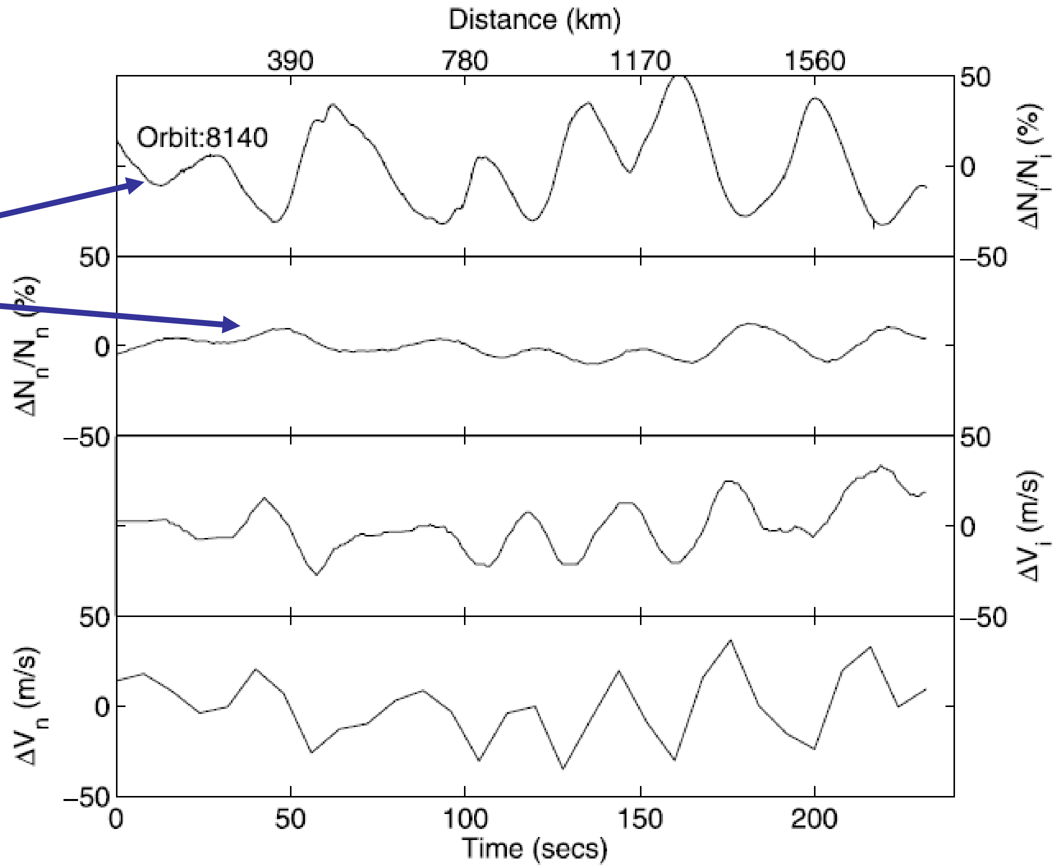

TID

GW

Figure 2. The top two panels show the ion (see Figure 1) and neutral density perturbations for orbit 8140, respectively. The third and fourth panels display the corresponding linearly detrended ion and neutral vertical velocities.

What are Gravity Waves?

- Gravity waves are buoyancy waves – the restoring force comes from Archimedes's principle.
- They involve vertical displacement of air parcels, along slanted paths
- The waves are transverse with temperature and wind pertubations, δT and δw being the two free parameters that oscillate for a freely propagating wave
- They are found everywhere in the atmosphere
- They can propagate vertically and horizontally, transporting momentum from their source to their sink
- Global circulation models use GW parameterization schemes to represent GW transfer of momentum - major source of controversy

Atmospheric Gravity Waves

- Ubiquitous
- Small scale
- Wavelengths :

  tens to thousands km
- Periods: mins to hrs

Post-Sunset Enhancement of Eastward Electric Field

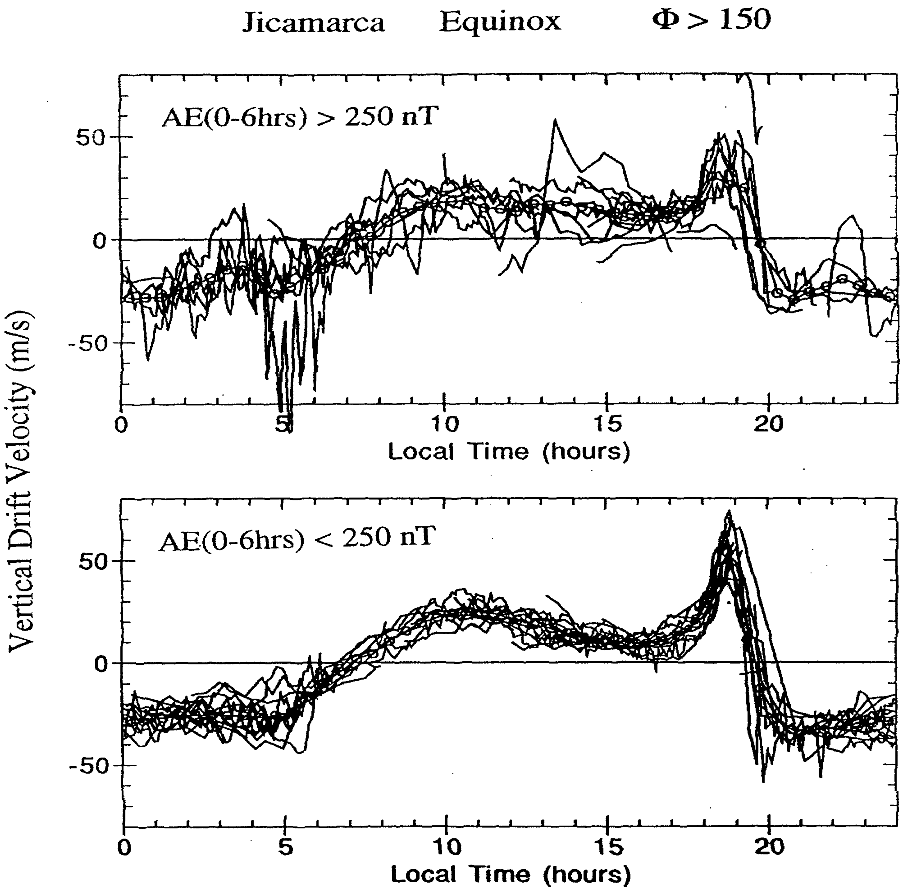

Superimposed plots of a large number of individual 24-hour measurements of vertical drifts at Jicamarca, Peru, showing the post-sunset or the pre-reversal enhancement of the eastward electric field. Data correspond to equinox solar maximum conditions for extended magnetic quiet (lower plot) and disturbed (upper plot) periods [From *Fejer et al.*, 1999].

F-region Dynamo

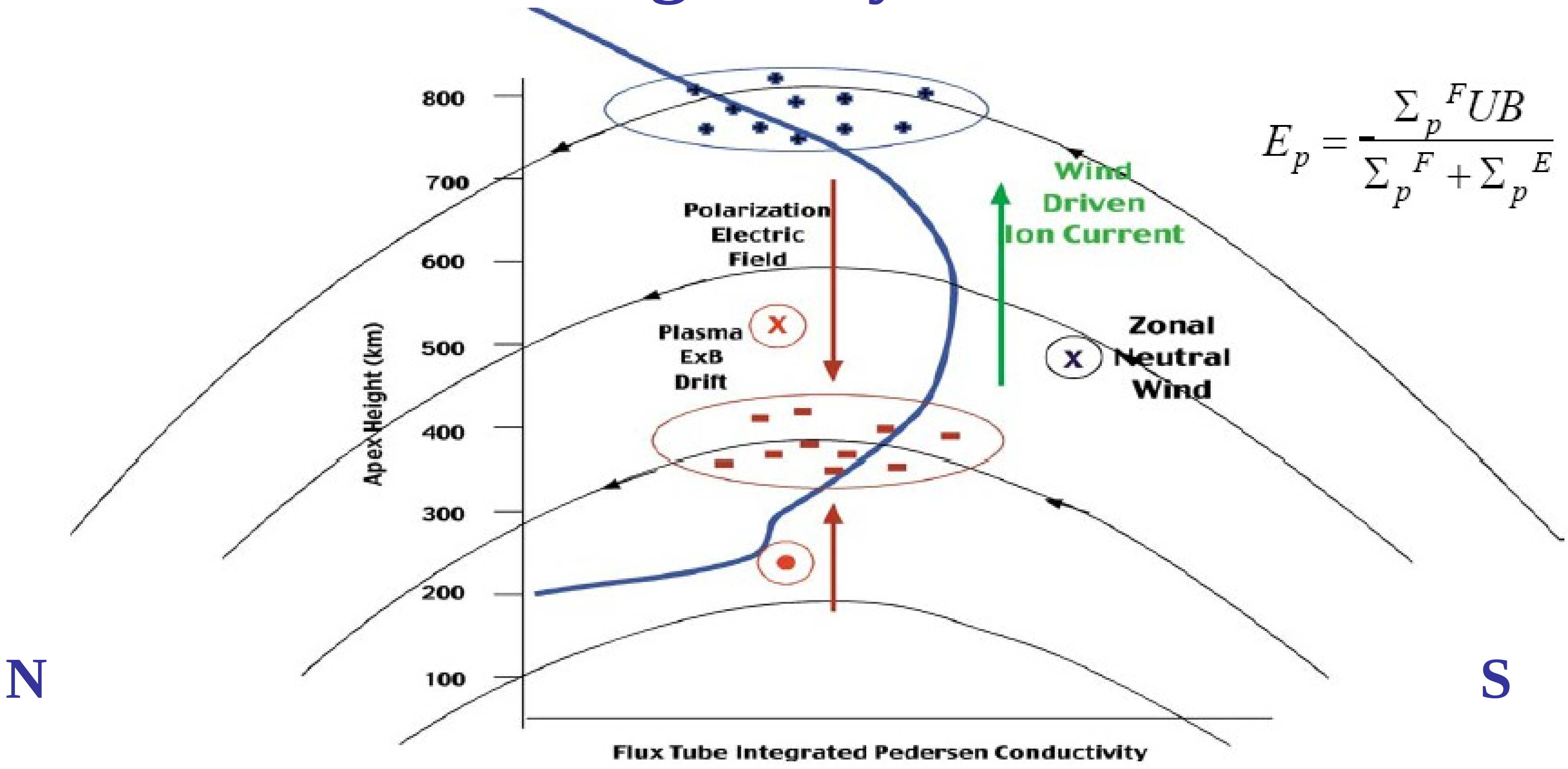

$$E_p = -\frac{\Sigma_p{}^F UB}{\Sigma_p{}^F + \Sigma_p{}^E}$$

F-region polarization electric field drives plasma eastward near the peak and above. But, the drift will be westward much below the peak. During the day E_p will be very small; during the night is close to $U \times B$

Electrodynamics of Pre-reversal enhancement

E field driven by zonal wind maps to an equatorward meridional E-region field.

W

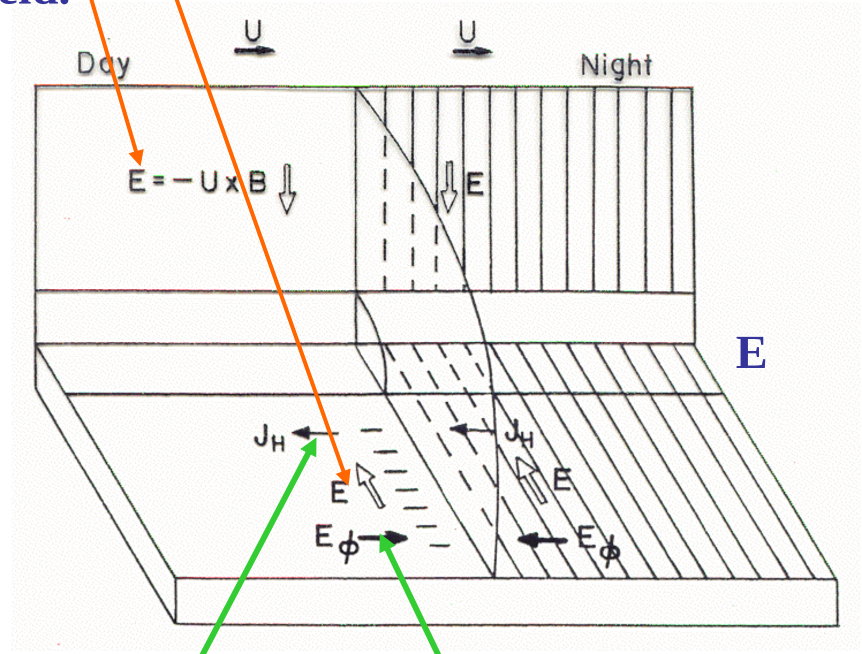

E

The E-region E field drives a westward Hall current, which is weak in the night side. The current difference produces negative charges in the day-night boundary and a new zonal E field that creates the PRE.

Farley et al, JGR, 13723, 1986

Post-sunset Vortex of F-region Plasma Drifts

Drift measurements conducted at Jicamarca on April 08, 1997.

The Vortex is characterized by upward and downward flows to the west and to the east and eastward and westward flows on the top and the bottom respectively.

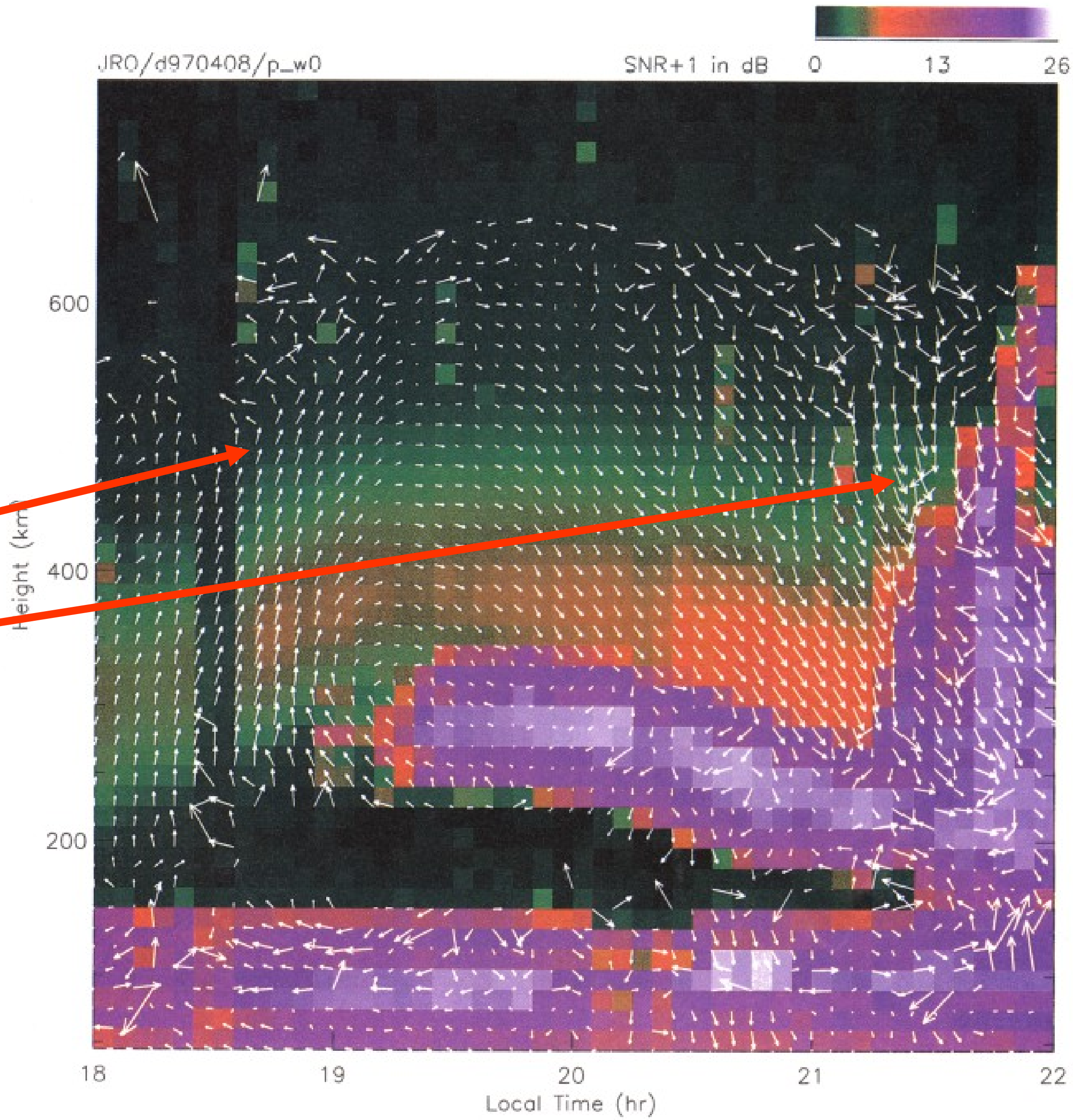

Kudeki and Bhattacharyya, JGR, 28163, 1999

Kudeki et al. (2007) JASTP

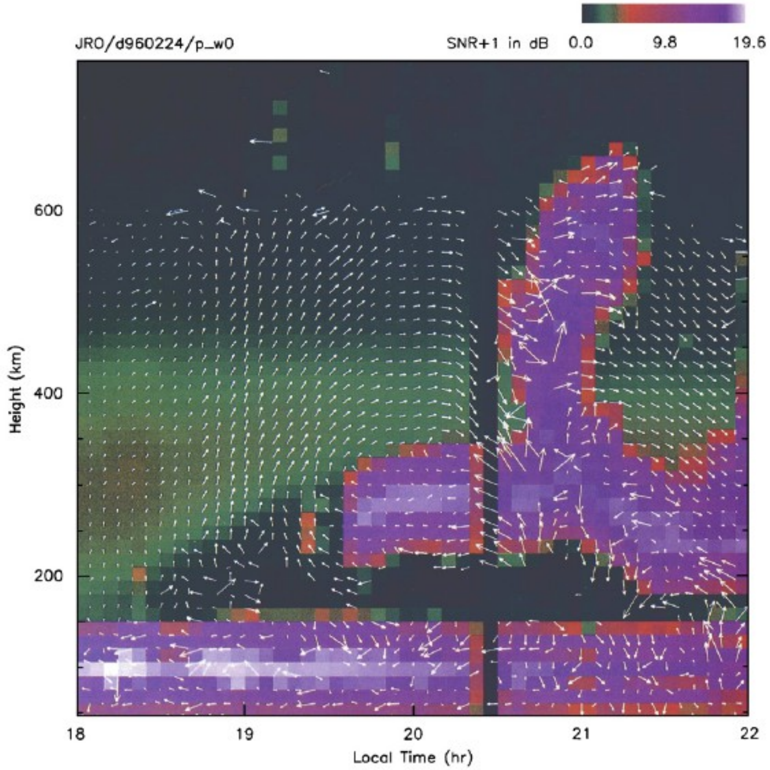

Kudeki et al. [2007] numerical simulation demonstrated that for values of the zonal wind equal to 200 m/s and gradient scale length of 20 km, the preferred scale size of the perturbation was 40 km and the growth rate equal to 200 sec, many times higher than the RT growth rate.

Sketch of the wind driven gradient drift (ExB) instability. The eastward wind drives an upward Pedersen current that polarizes the density perturbations that have westward tilted wave-fronts.

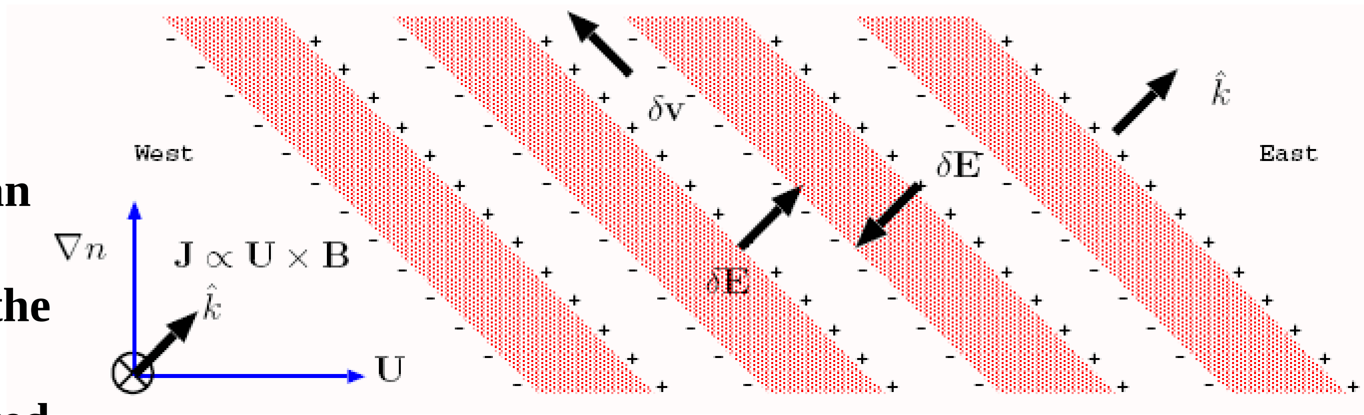

Vortex and ESF observations at JRO

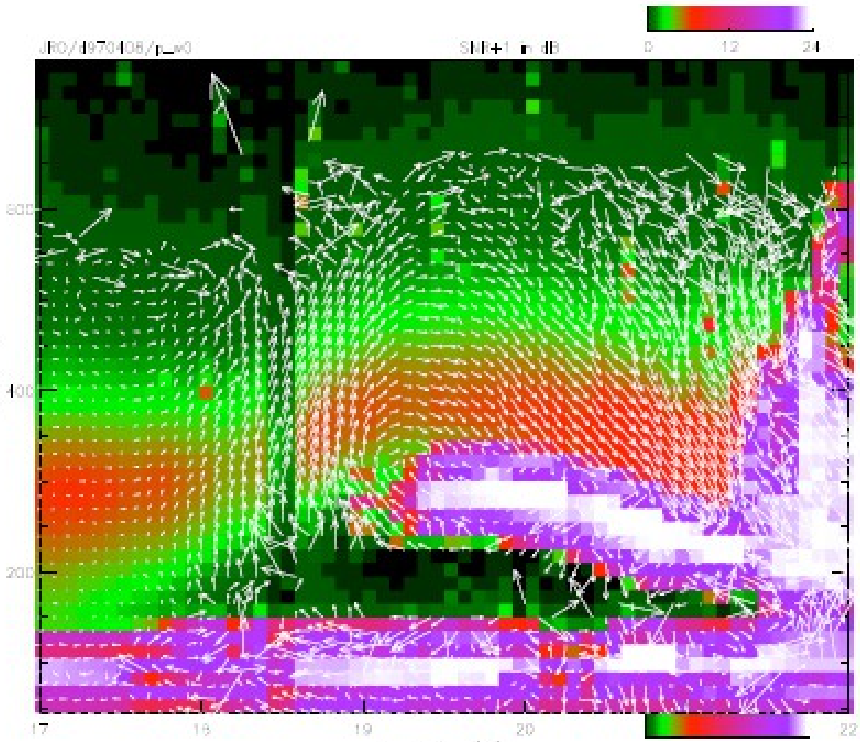 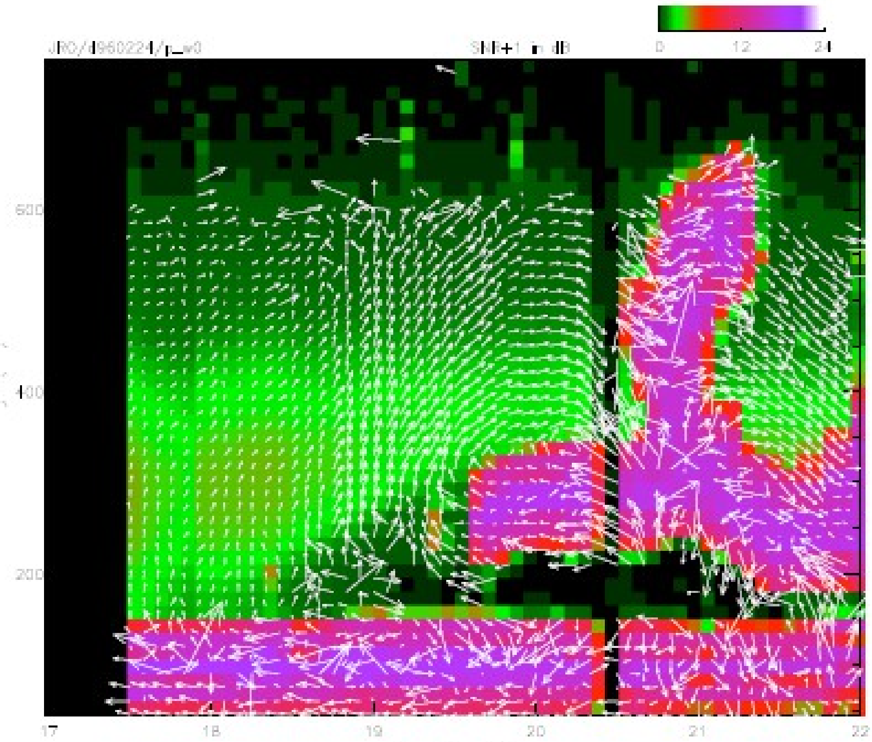

Sheared zonal flows in the post-sunset equatorial F region were known since the early 80’s, but the new high resolution JRO observations have shown that: (1) Equatorial Spread F develops within the sheared flow structure. (2) The shear is part of the post-sunset F-region vortex. It is possible that vortex fragmentation seeds the initiation of ESF.

Collisional Shear Instability (Hysell and Kudeki, 2004)

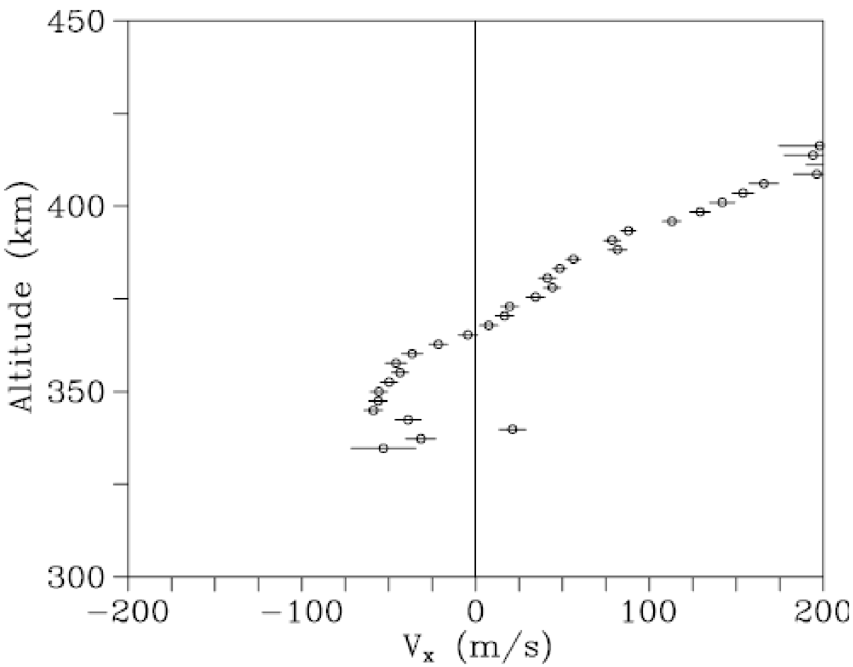

The Kelvin-Helmholtz instability in the collisional regimen predicts a long growth rate (50 min) with an initial wavelength of 30 km. Radar imagery reveals periodic distributions of bottom-type layer irregularities.

Jicamarca Interferometry observations

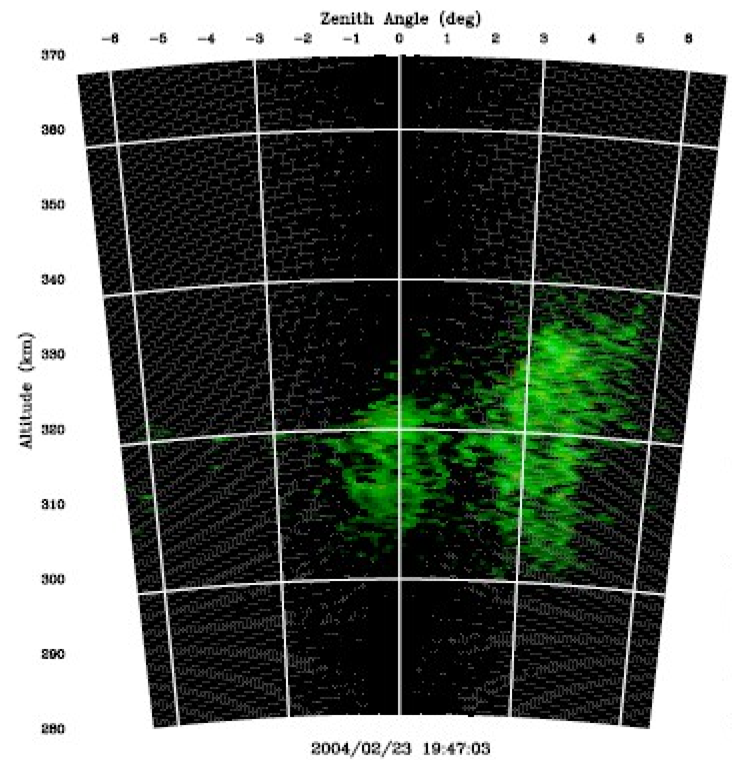

A snapshot in longitude and height

Large-Scale Wave structures (Tsunoda, GRL, 2006)

Diagram showing the development of a polarization electric field along an altitude-modulated E_s region. The E field maps to the plane over the magnetic equator that produces a displacement of the F region, a LSWS

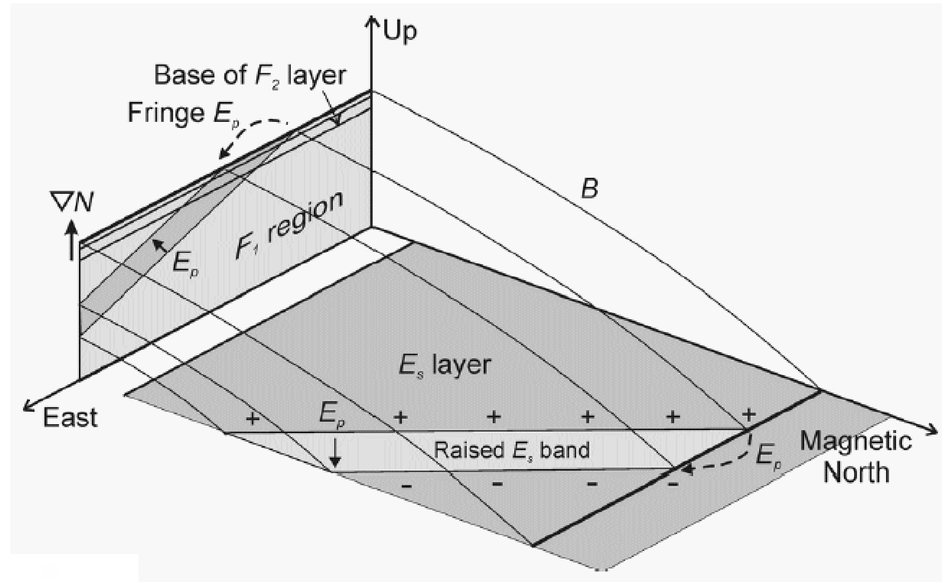

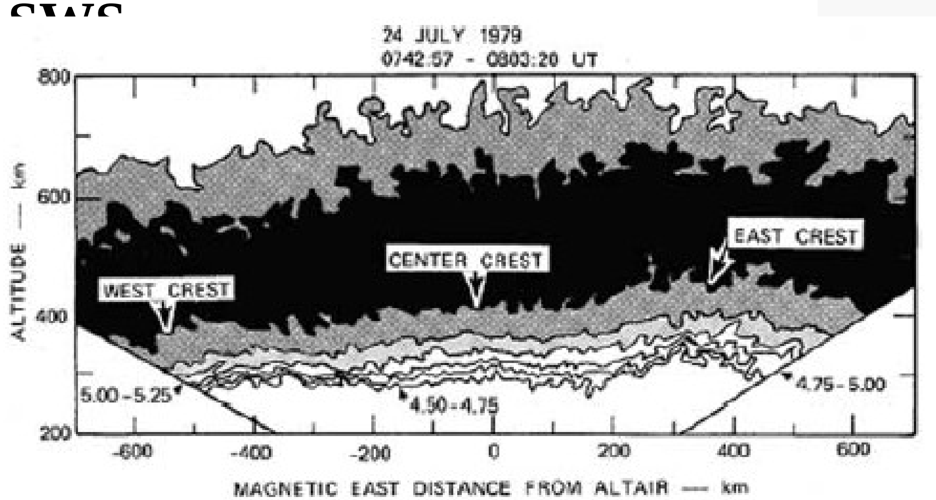

Density distributions measured during an east-to-west scan with the ALTAIR IS radar on 24 July 1979 {Tsunoda and White, 1981].

Tsunoda, GRL, 2006 (Large-Scale Wave structures)

Diagram showing the development of a polarization electric field along an altitude-modulated E_s region. The E field maps to the plane over the magnetic equator that produces a displacement of the F region, a LSWS.

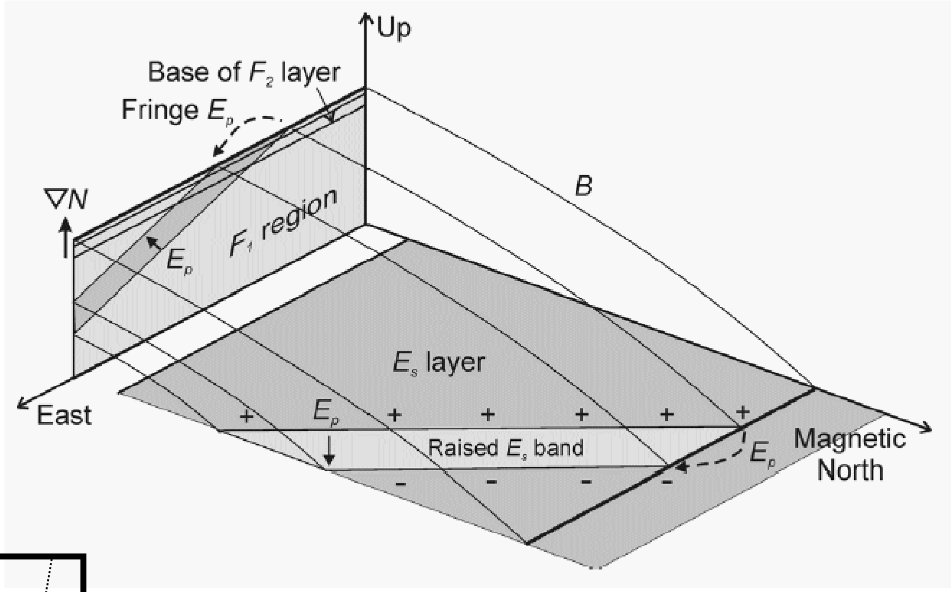

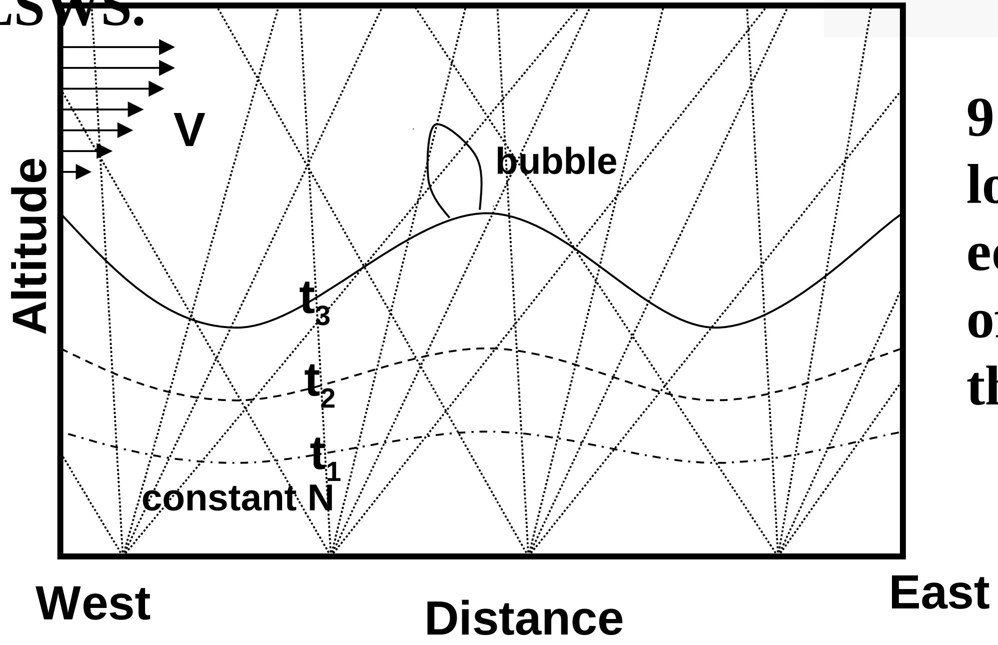

9 GPS receivers are presently located along the magnetic equator to observe the variability of TEC across Peru, Bolivia and the western part of Brazil.

BSS

Bottomside Sinusoidal irregularities (AE-E)

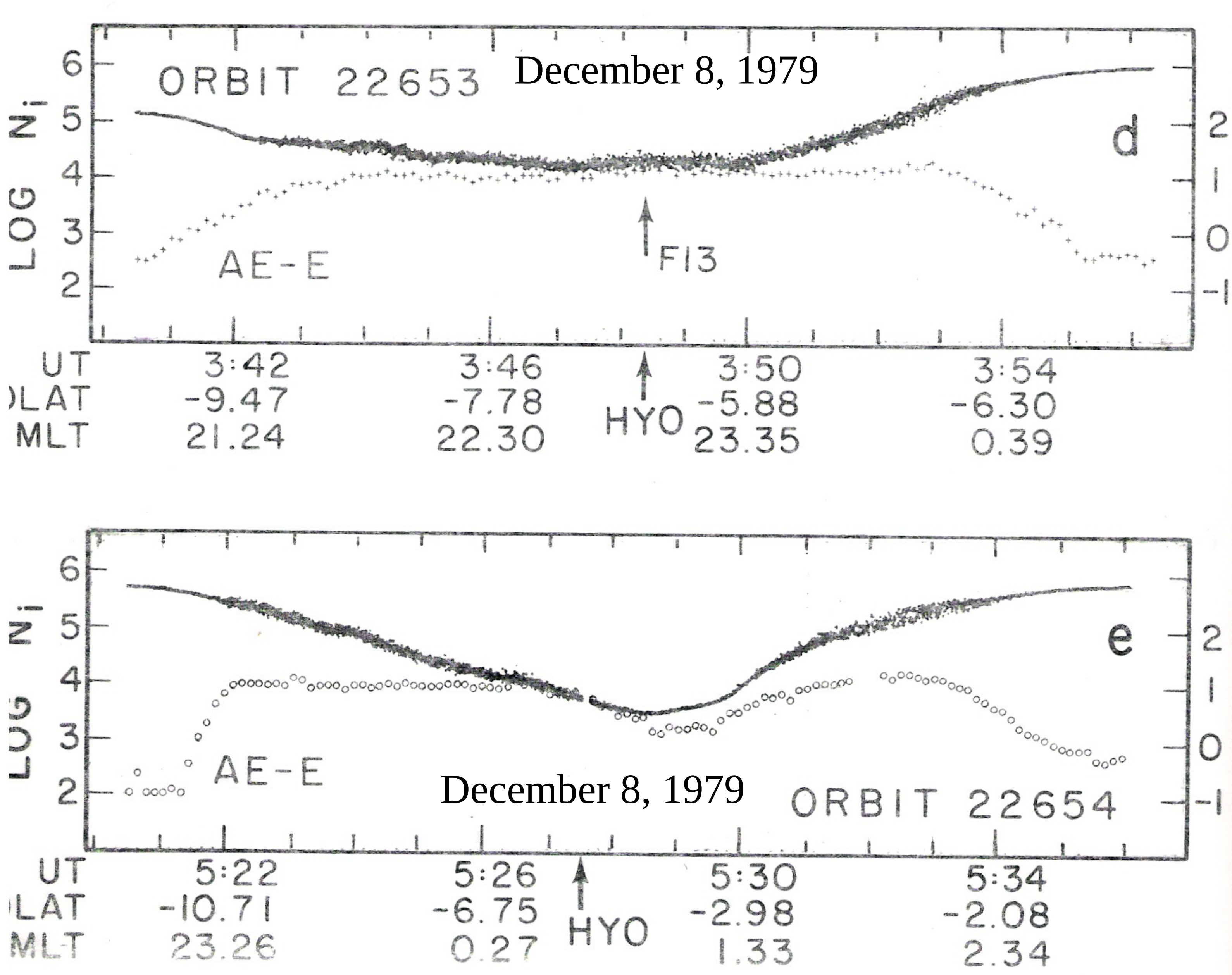

Bottomside Sinusoidal irregularities (AE-E)

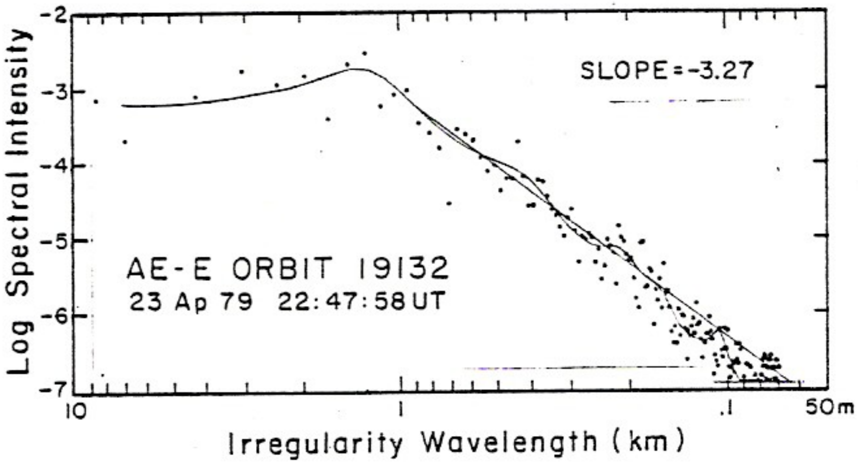

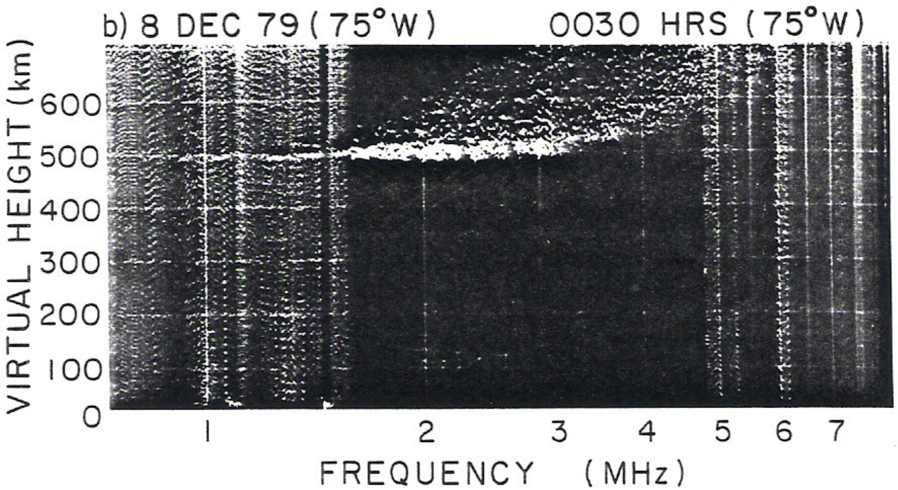

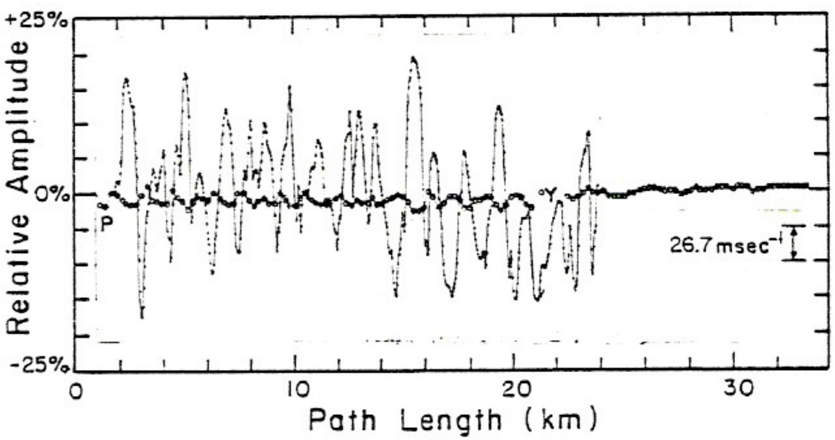

Frequency spread F ionograms observed at Huancayo during the time of AE-E overpasses.

Scale sizes vary between 3 km and 500 m

Observed only within 10° from magnetic equator

Valladares et al., JGR, 1983; Cragin et al., JGR, 1985

UHF Scintillations and Frequency-Type spread, November 10, 2002

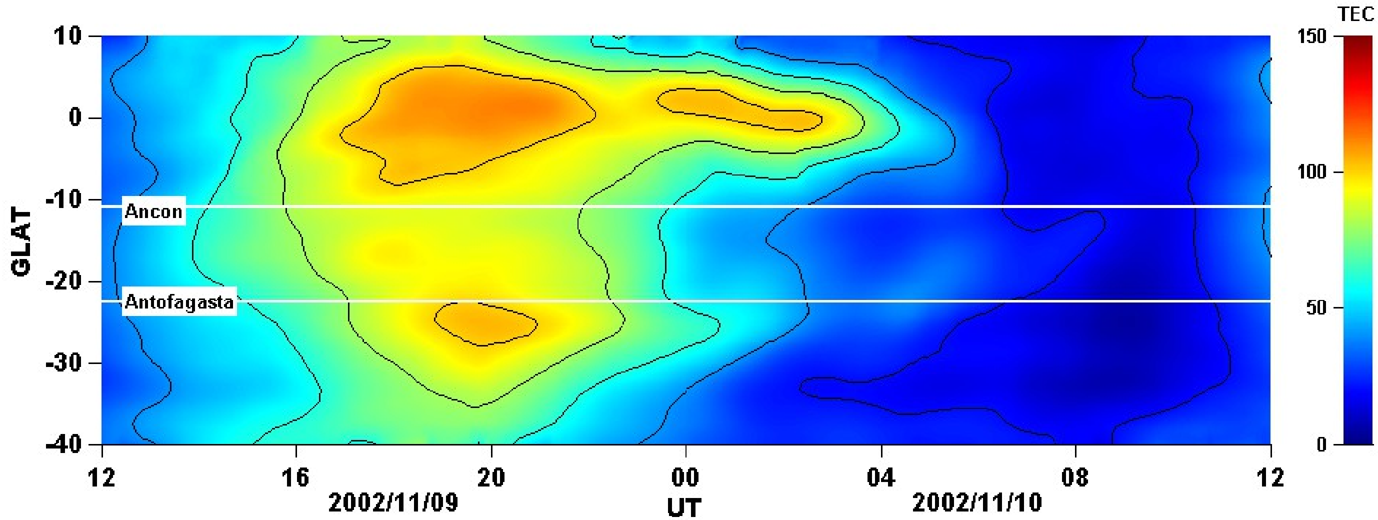

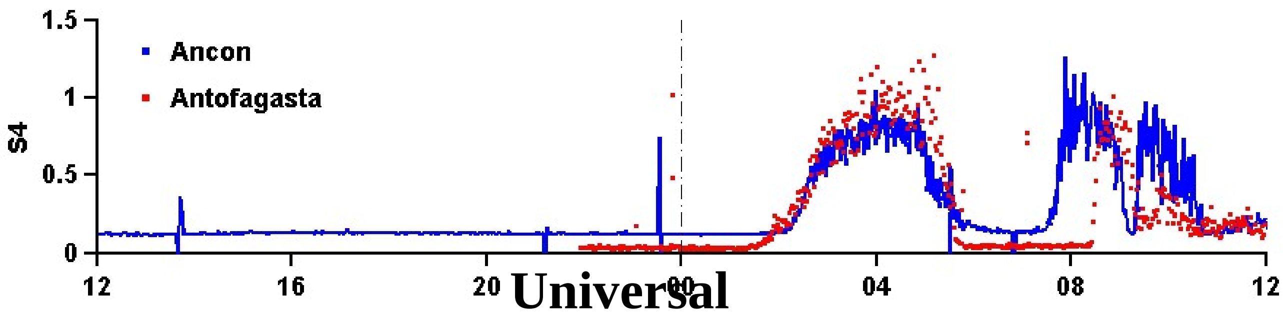

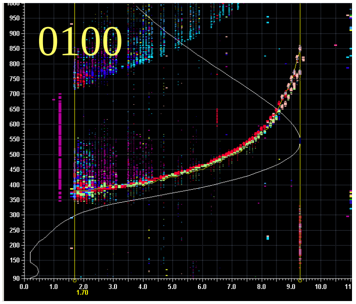

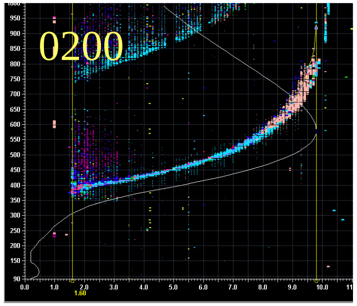

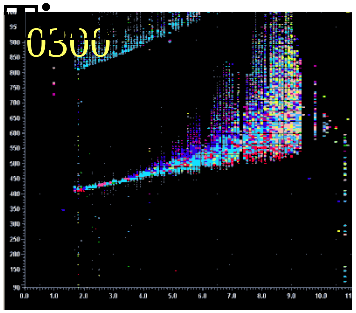

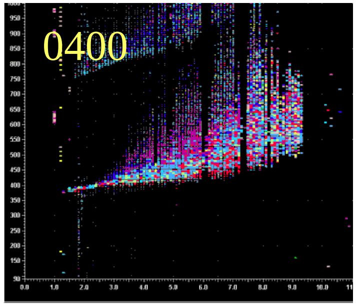

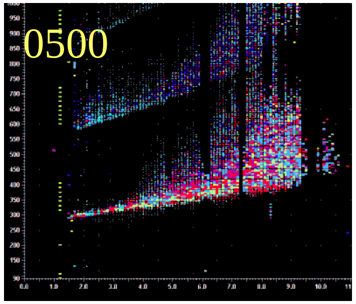

TEC, UHF Scintillation & Frequency-type ionograms, January 27, 2003

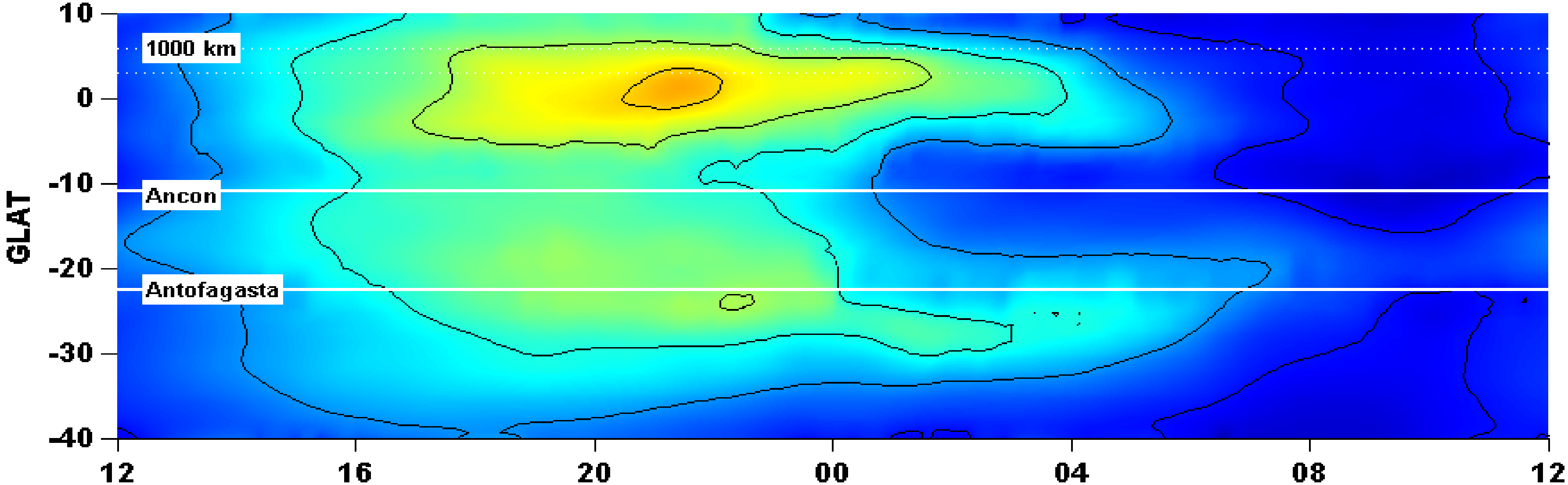

We have concluded that scintillations and frequency-type ionograms are due to the presence of BSS irregularities.

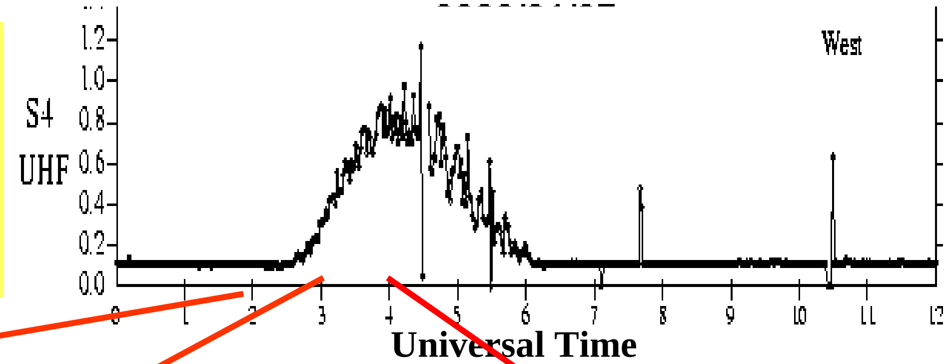

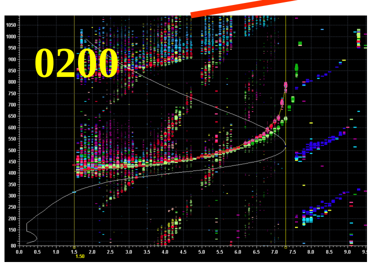

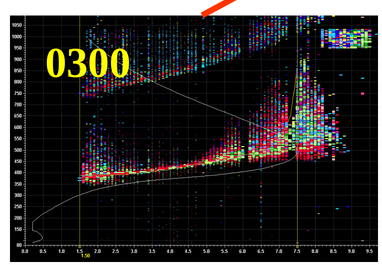

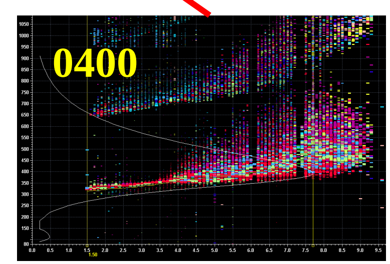

TEC and scintillations for December 21, 2002

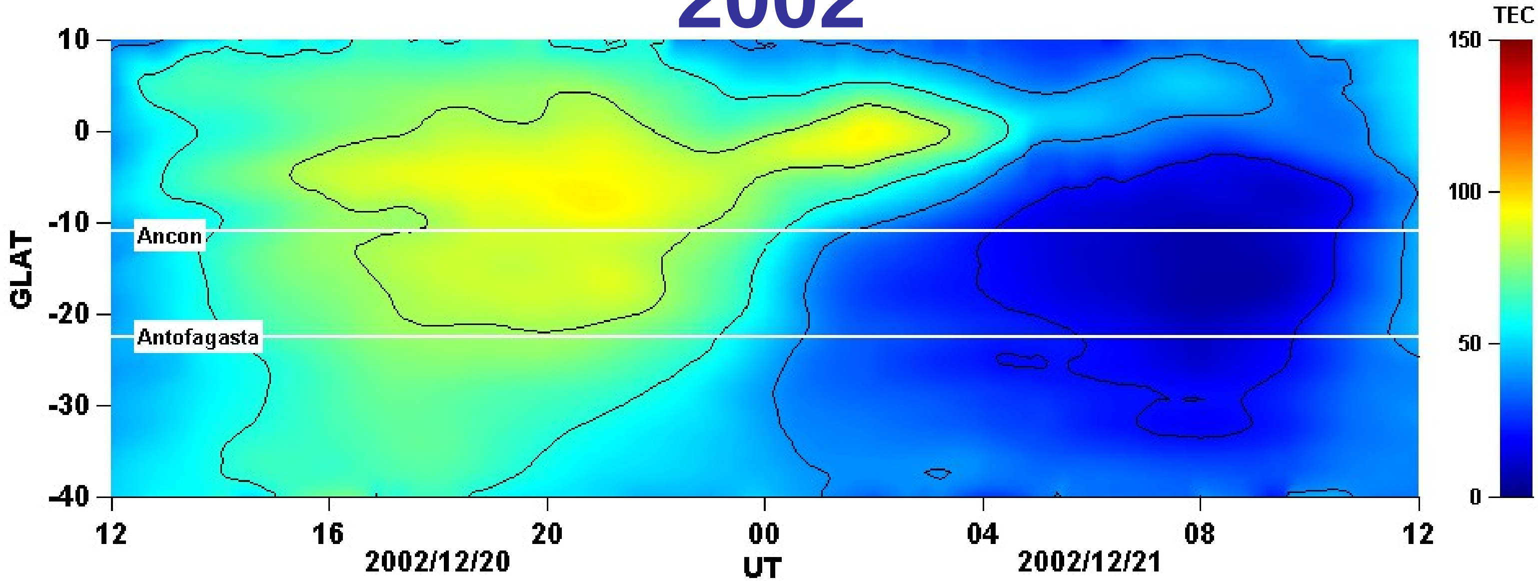

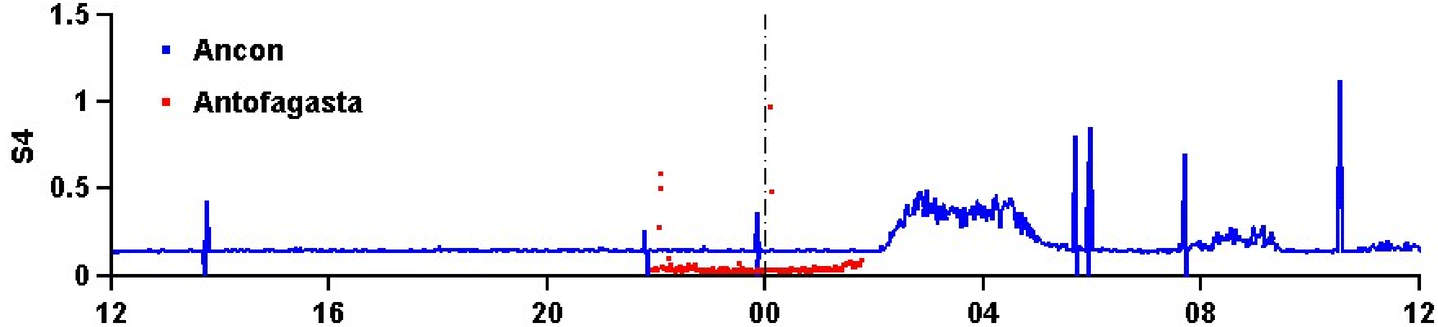

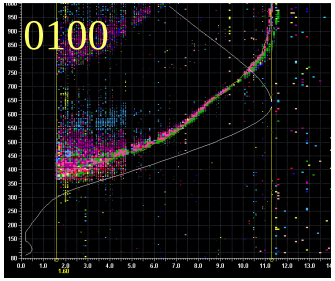

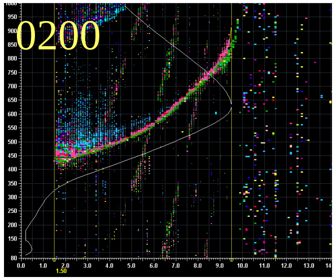

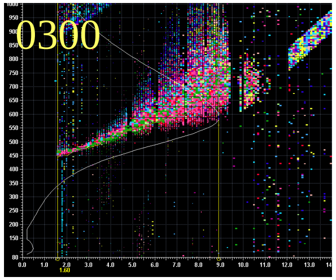

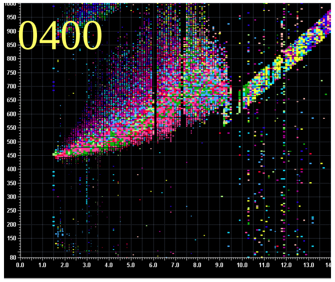

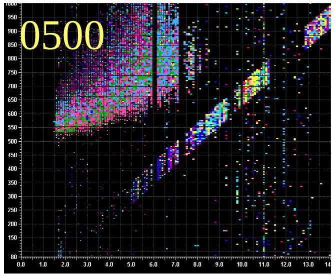

DMSP EPBs 1989 – 2002

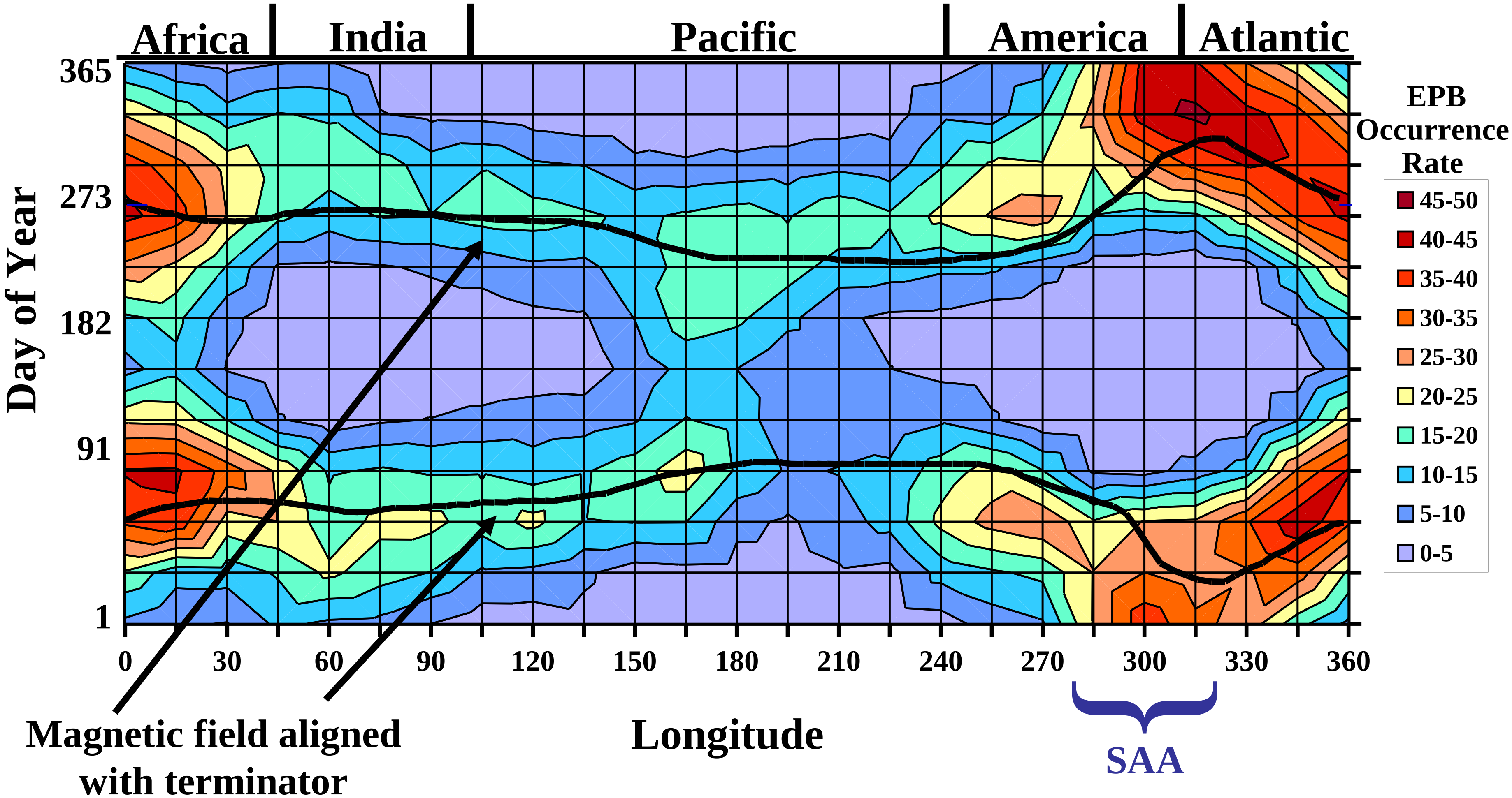

Solar-cycle averaged monthly rates of equatorial plasma bubbles encounter by DMSP (8300 bubbles). Longitudinal variability due to radiation belt precipitation that can enhance Σ_E and lower growth rate.

Burke et al., Annales Geophys, 2004

TEC depletions observed in November 07 and 08, 2008

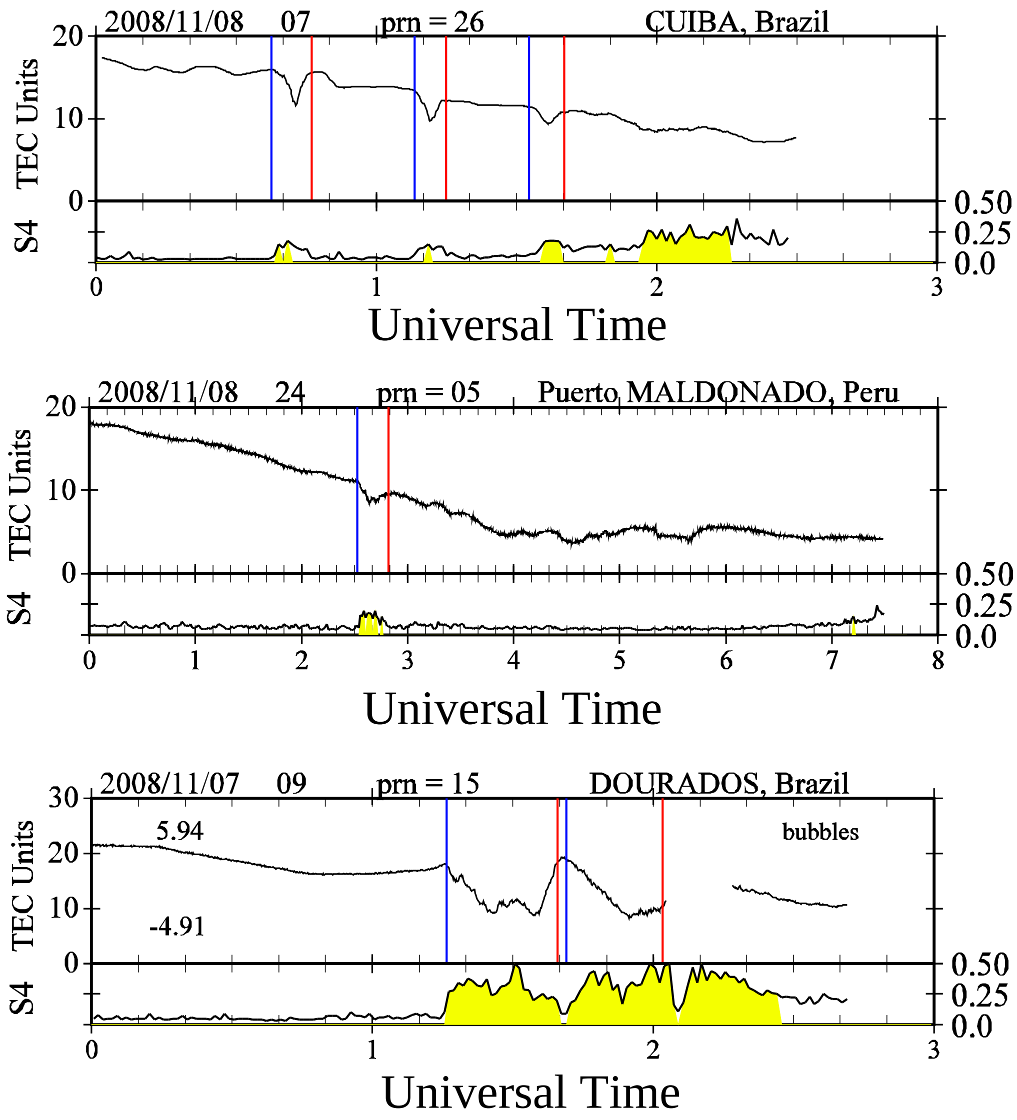

Seasonal Variability of TEC depletions (plasma bubbles)

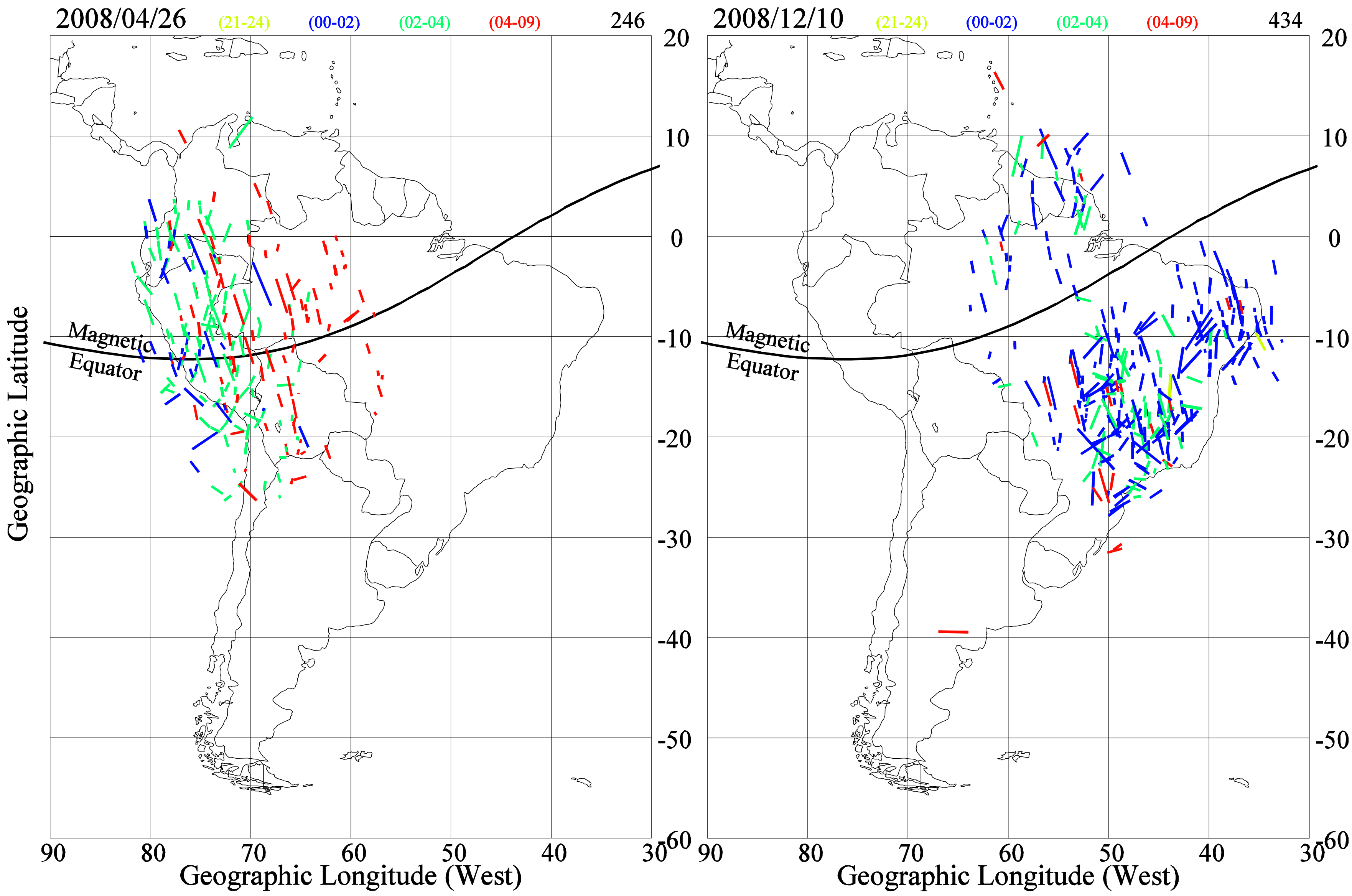

TEC Depletions on 2 Consecutive days (MCH 13-14, 2008)

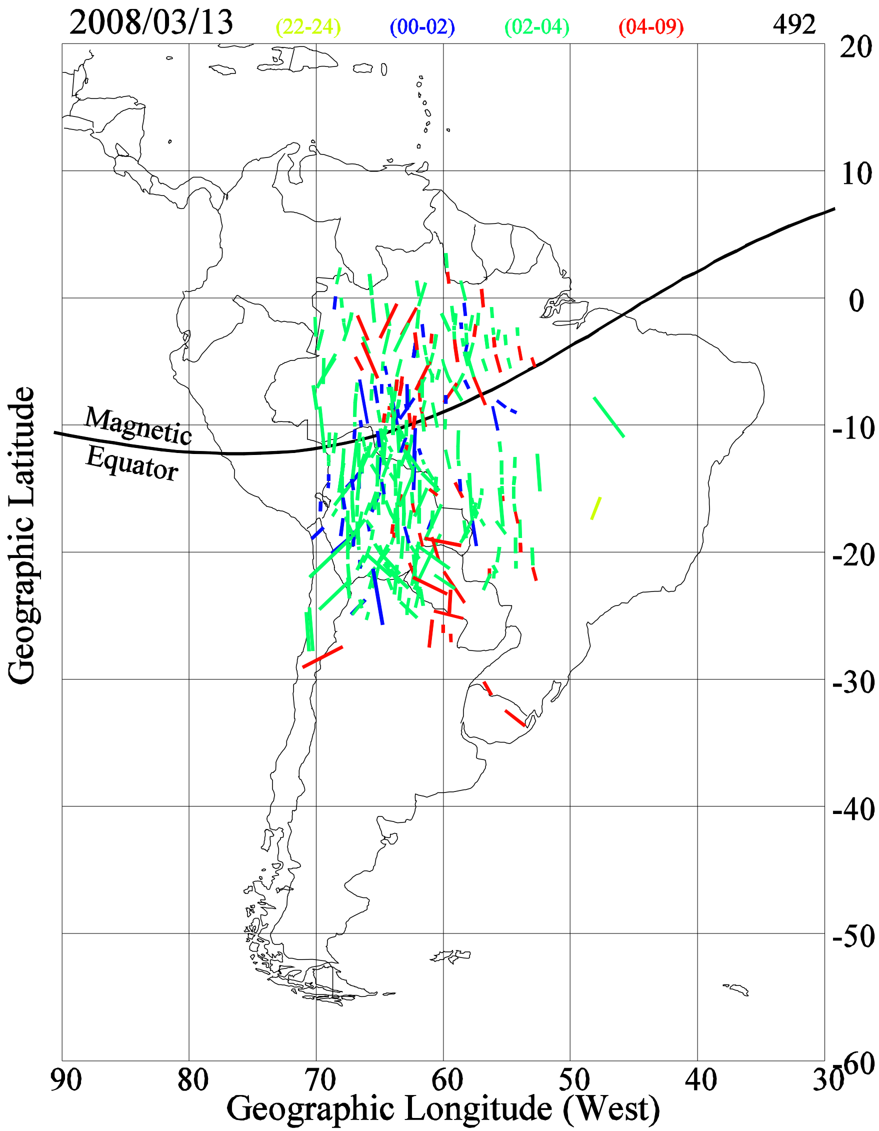

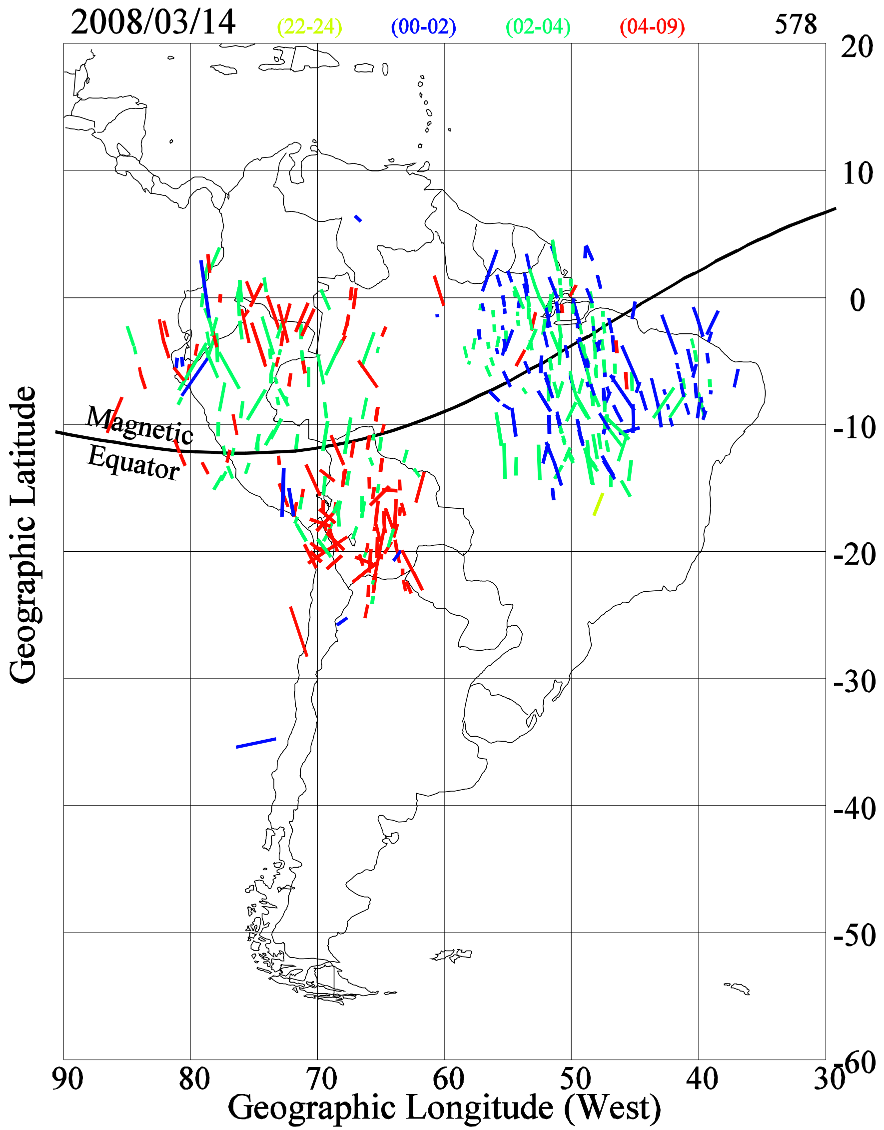

TEC Depletion on Mch 16, 2008

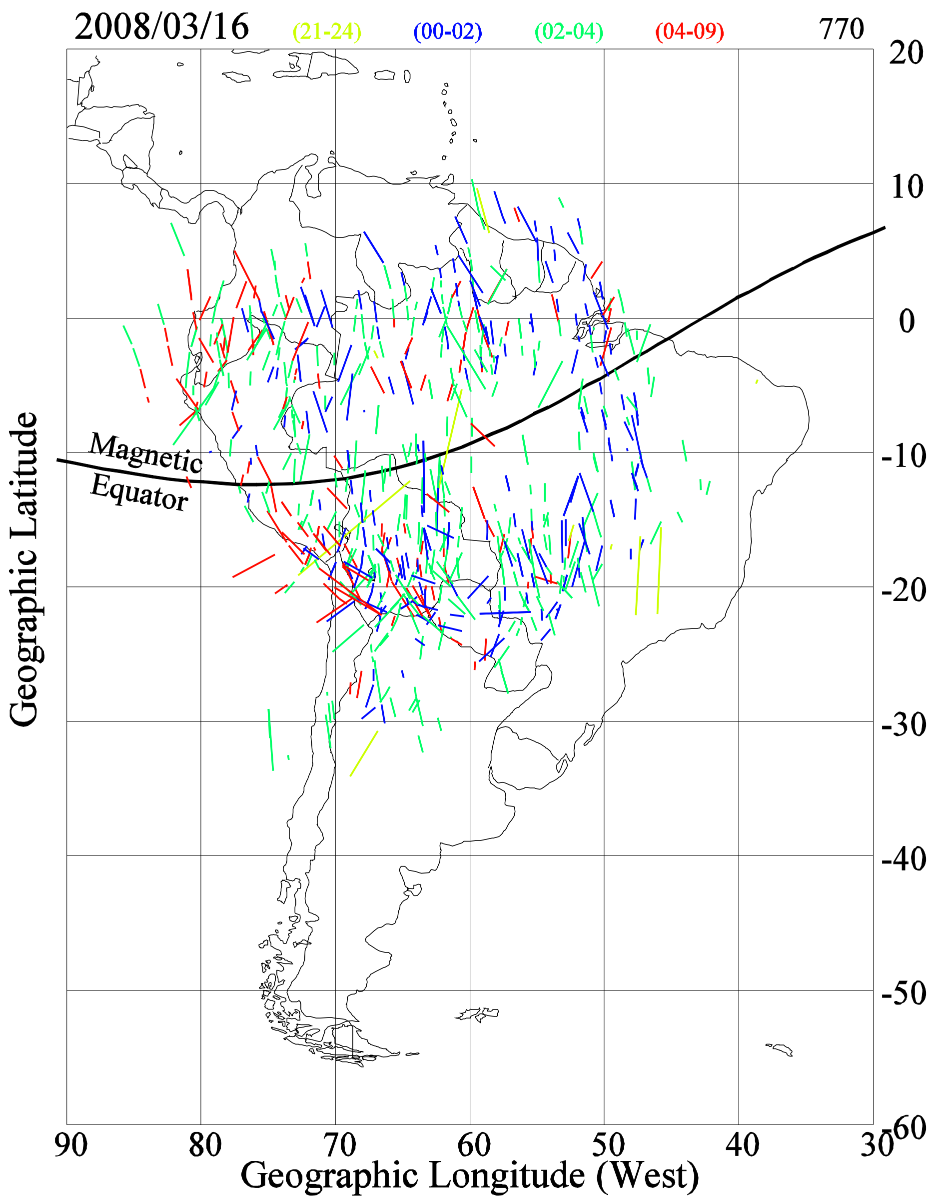

TEC depletions observed on April 25, 2008

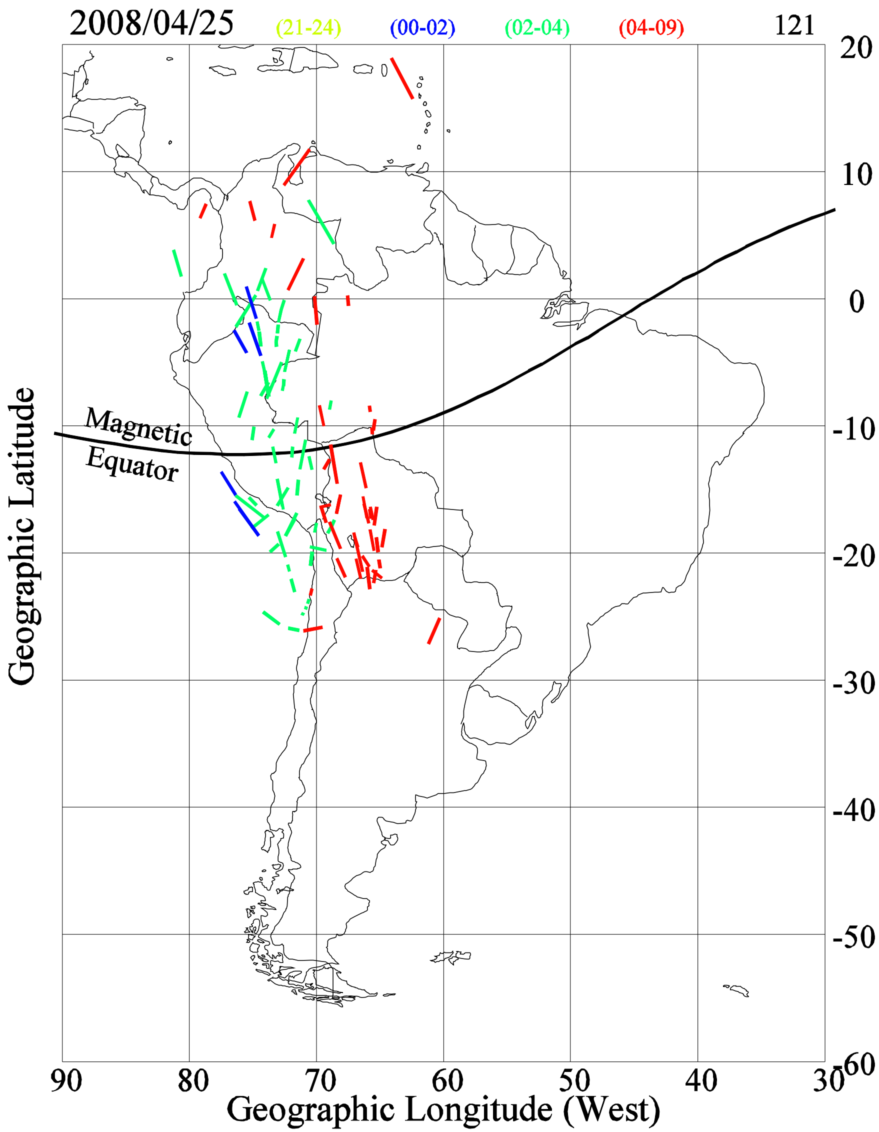

Same TEC depletions mapped to Eq. vs UT

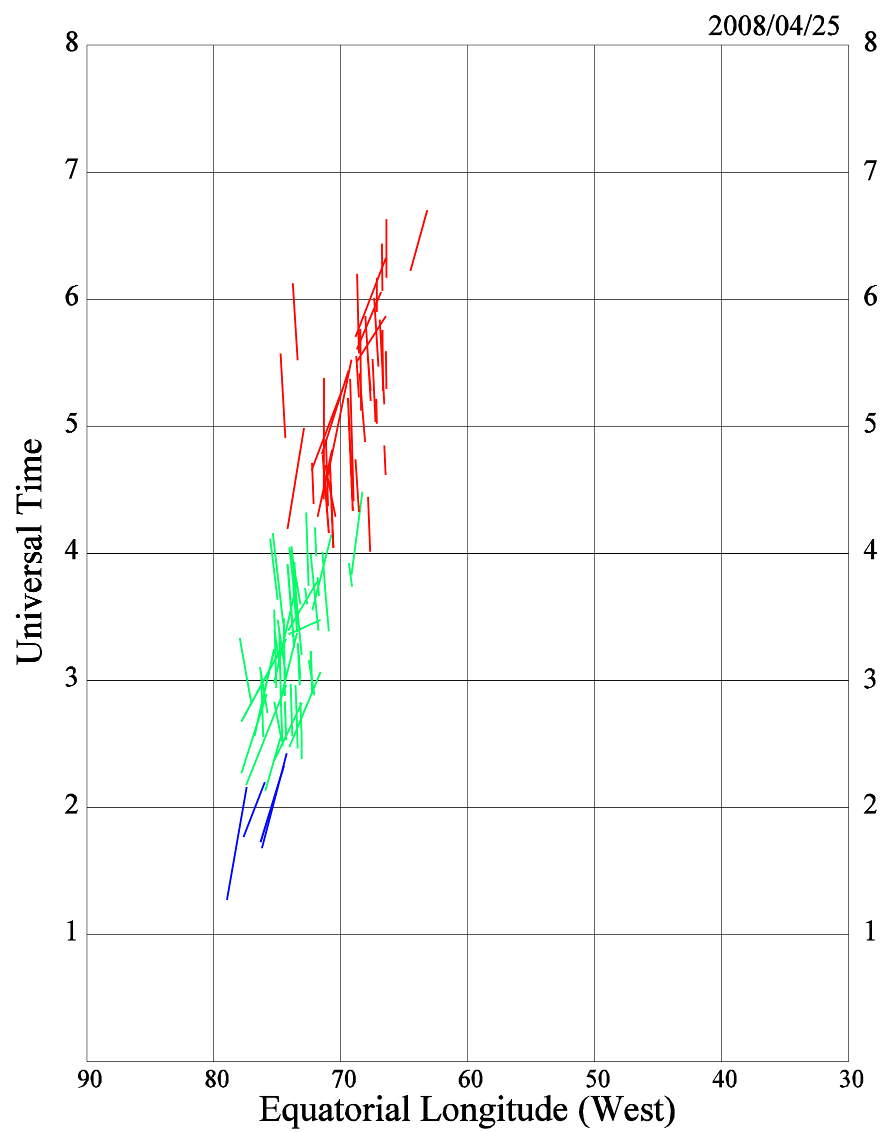

Total number of TEC depletions observed over South America in 2008

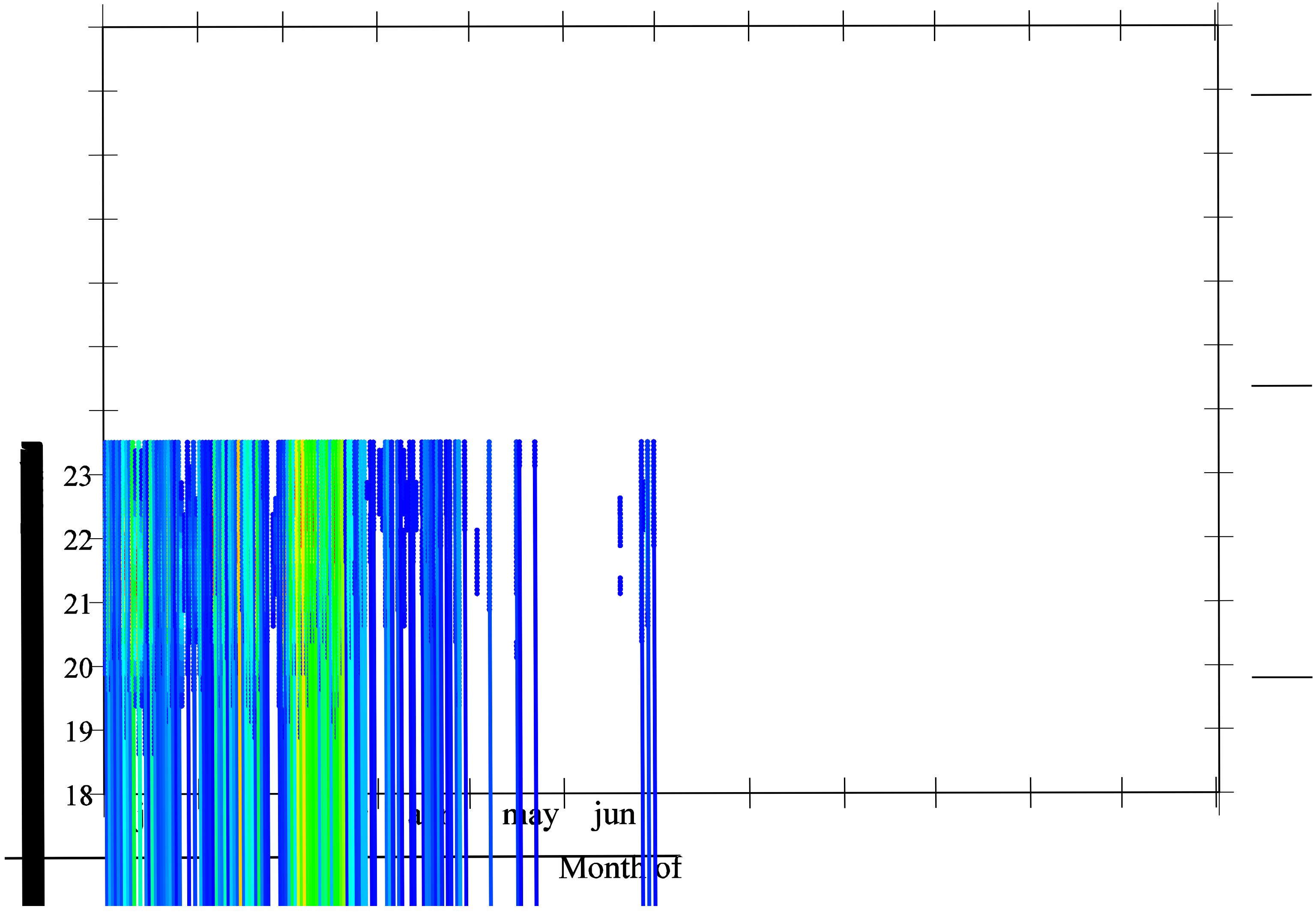

Total number of TEC depletions observed over South America in 2009

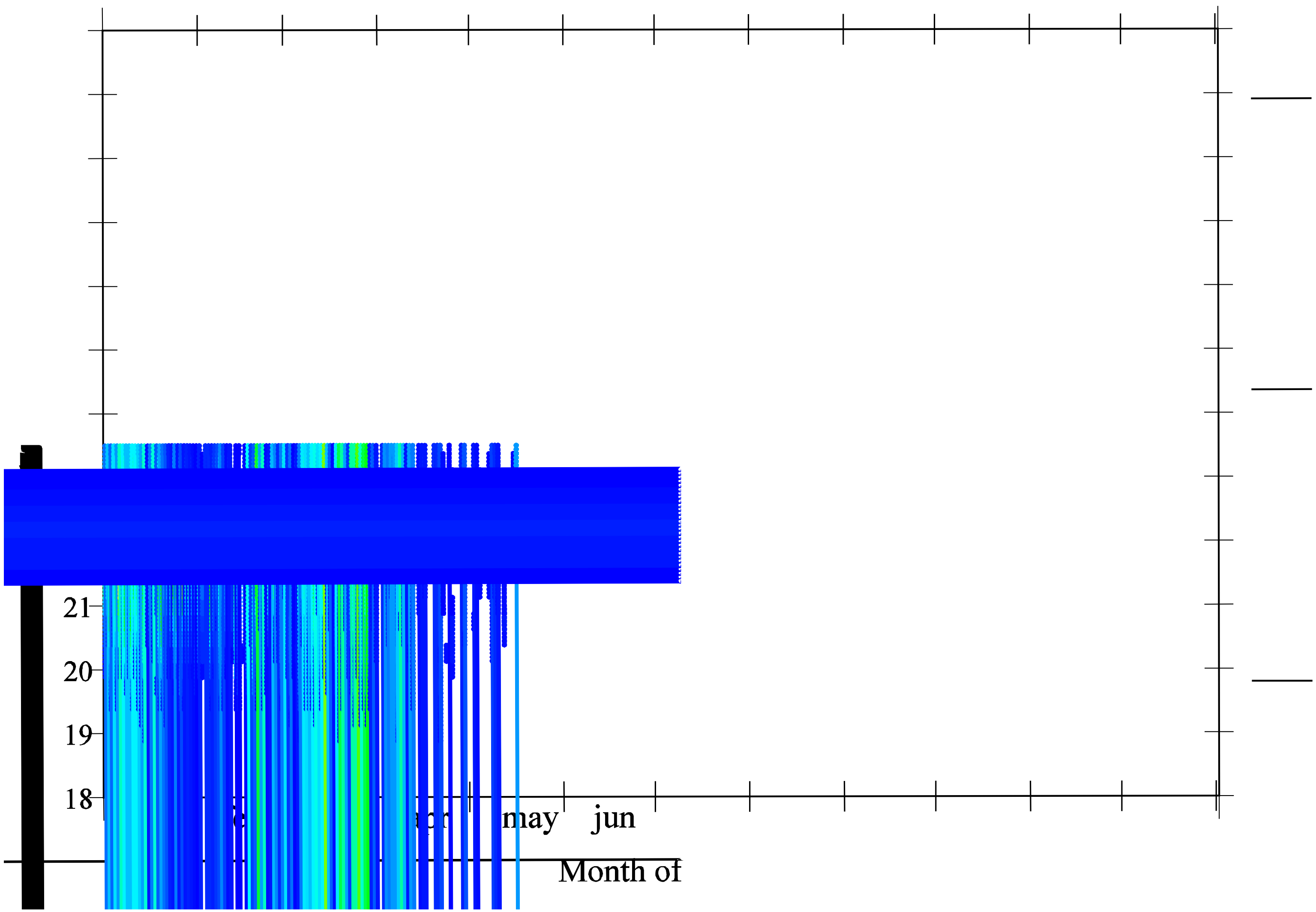

Total number of TEC depletions observed over South America in 2010

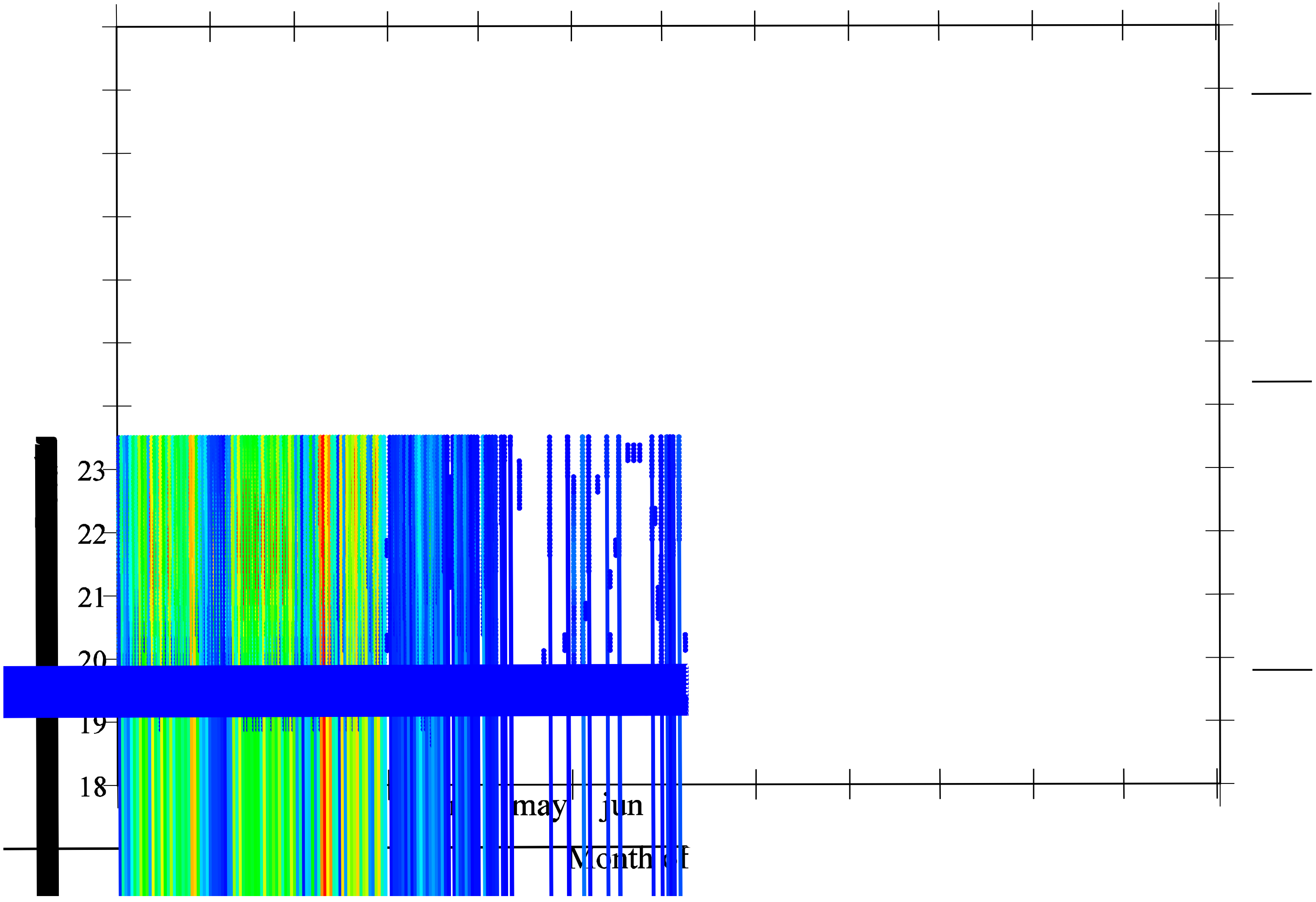

Total number of TEC depletions observed over South America in 2011

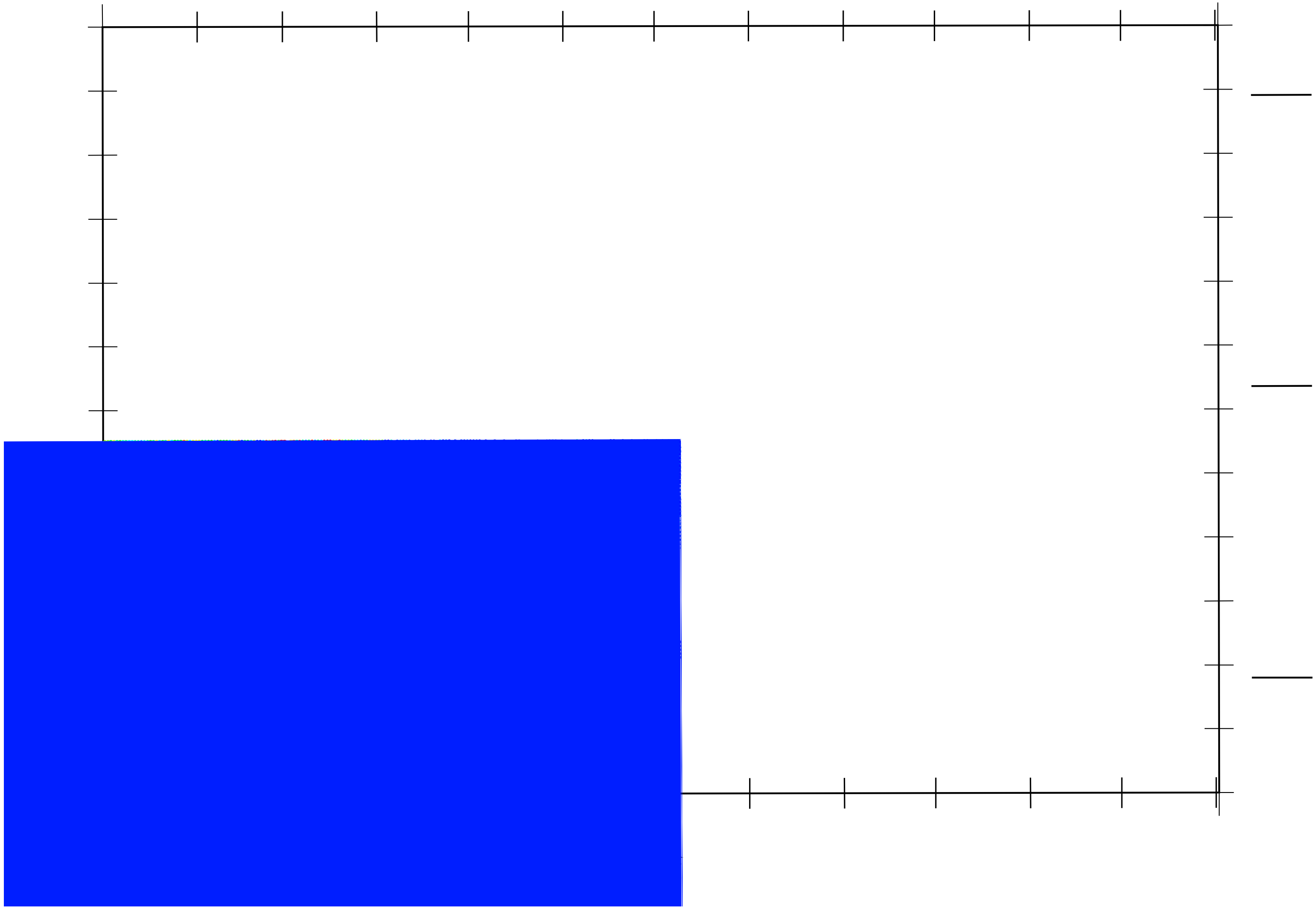

TEC depletions and TIDs in Two different sectors

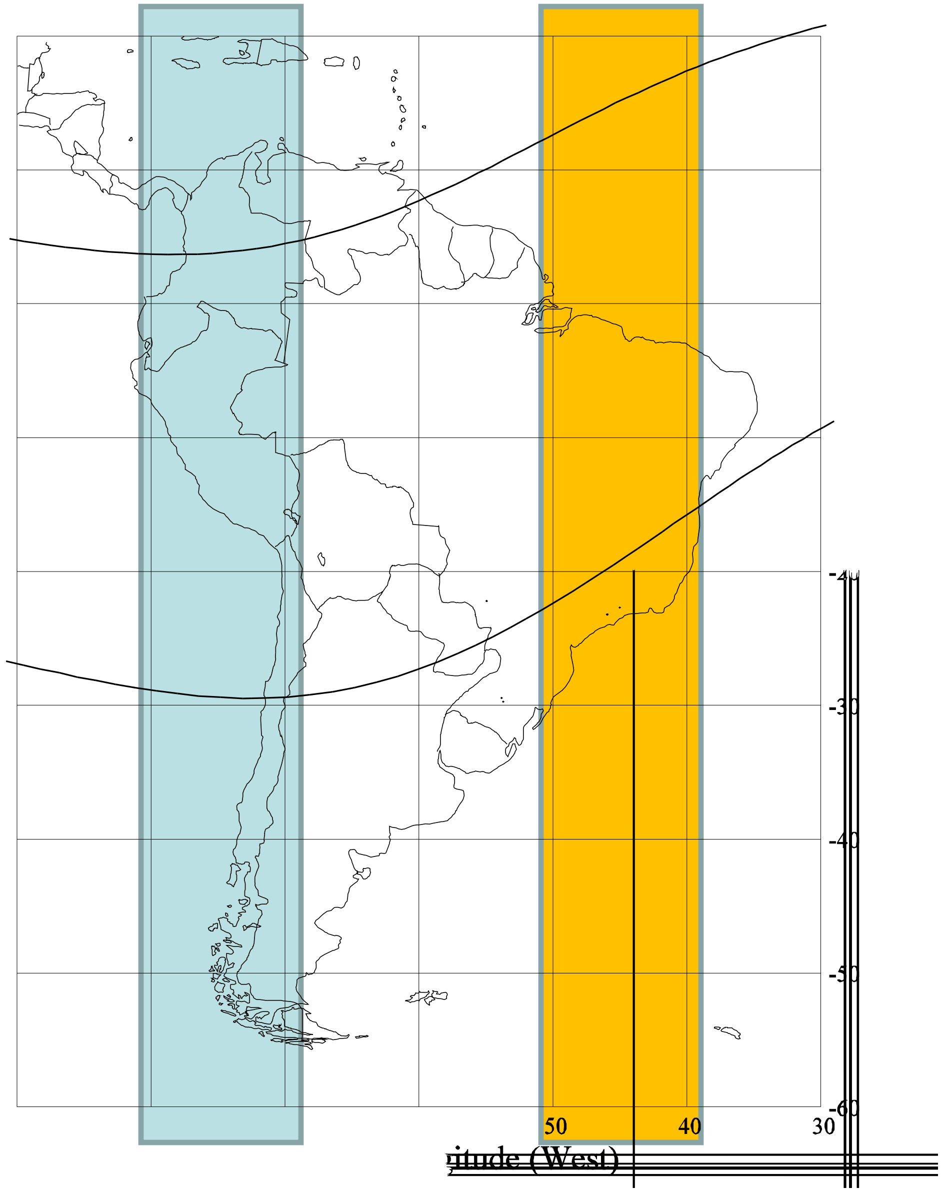

Number of TEC depletion detections as a function of Local time and day of Year between 80° and 70° W

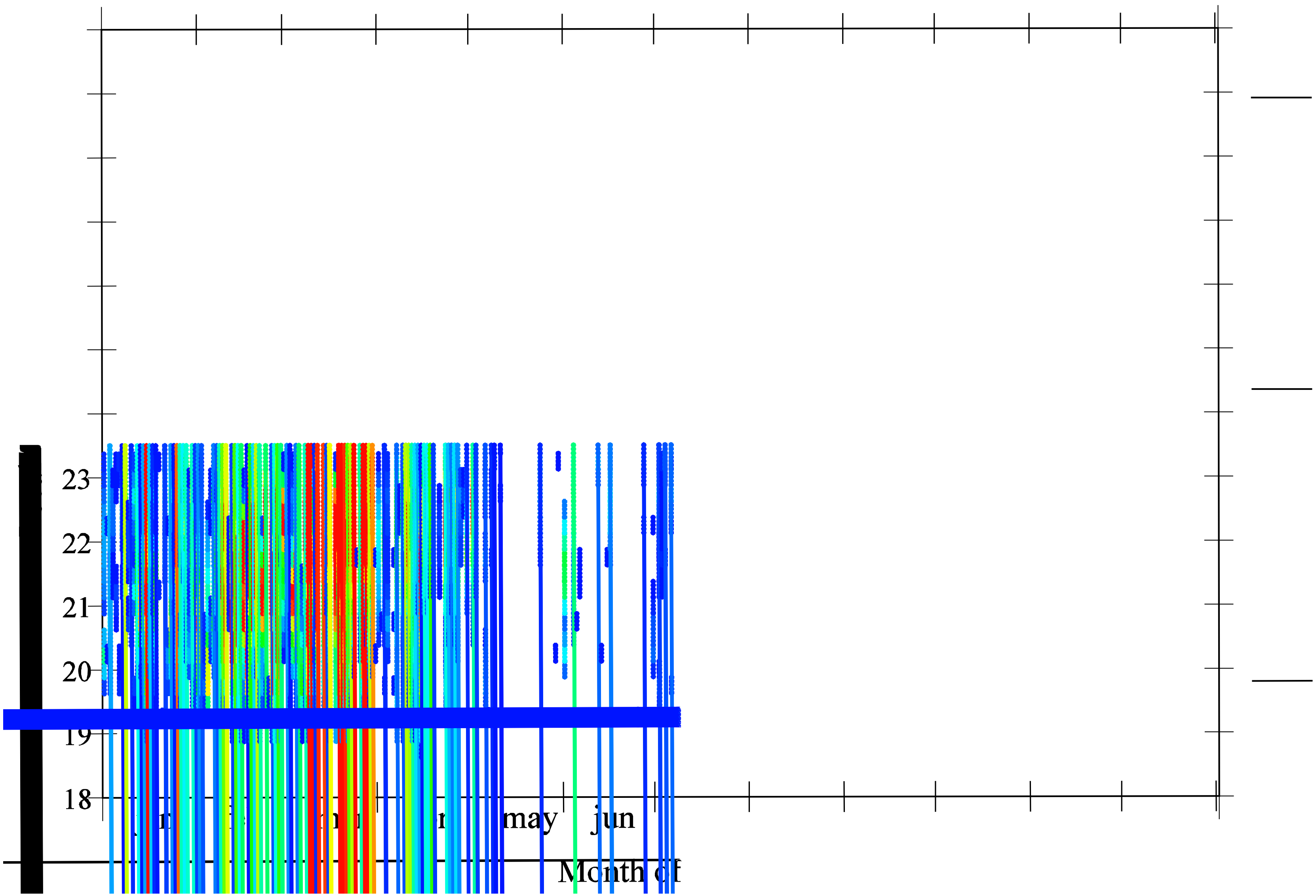

Number of TEC depletion detections as a function of Local time and day of Year between 50° and 40 ° W

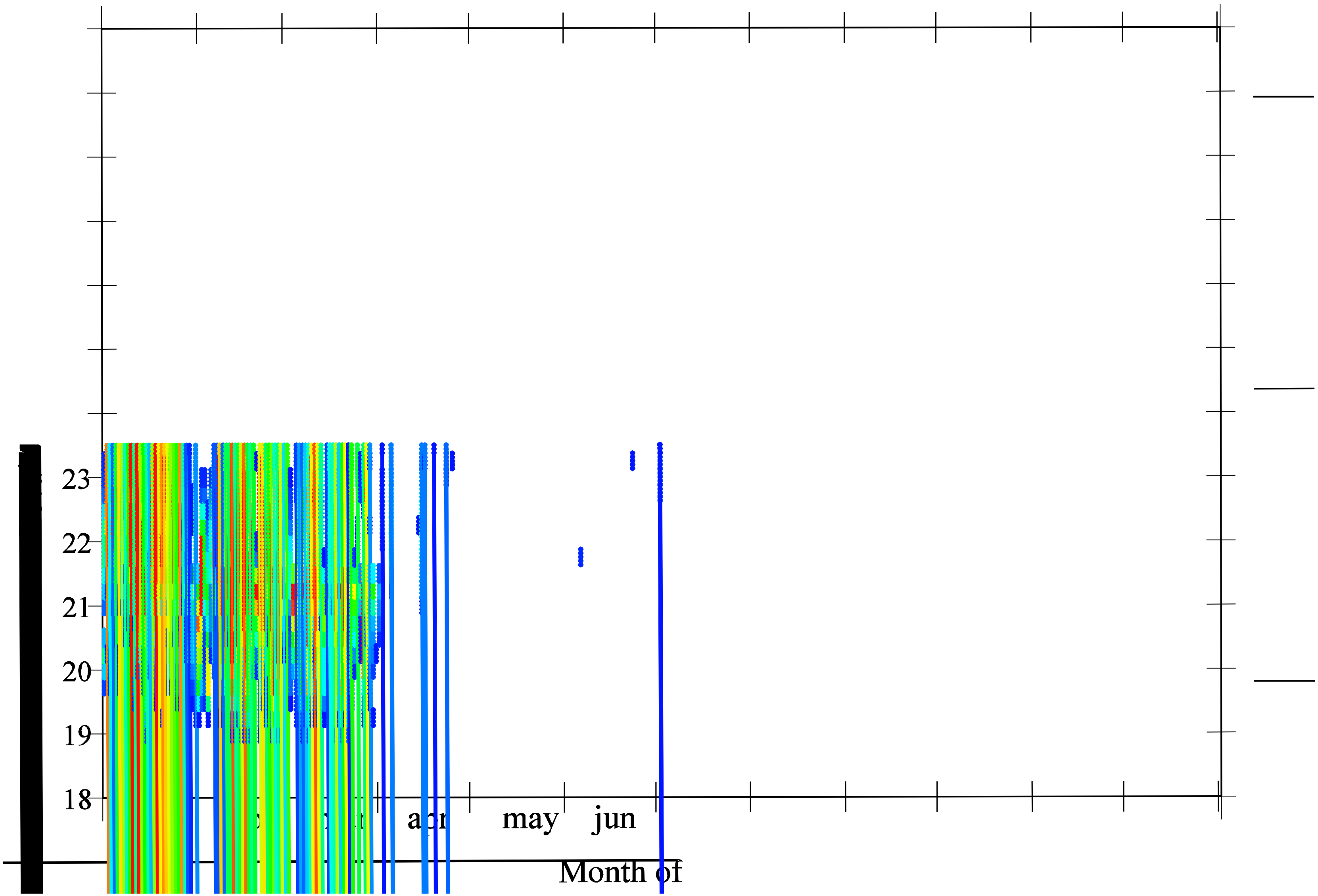

East-west width of TEC depletions for years 2010 and 2011

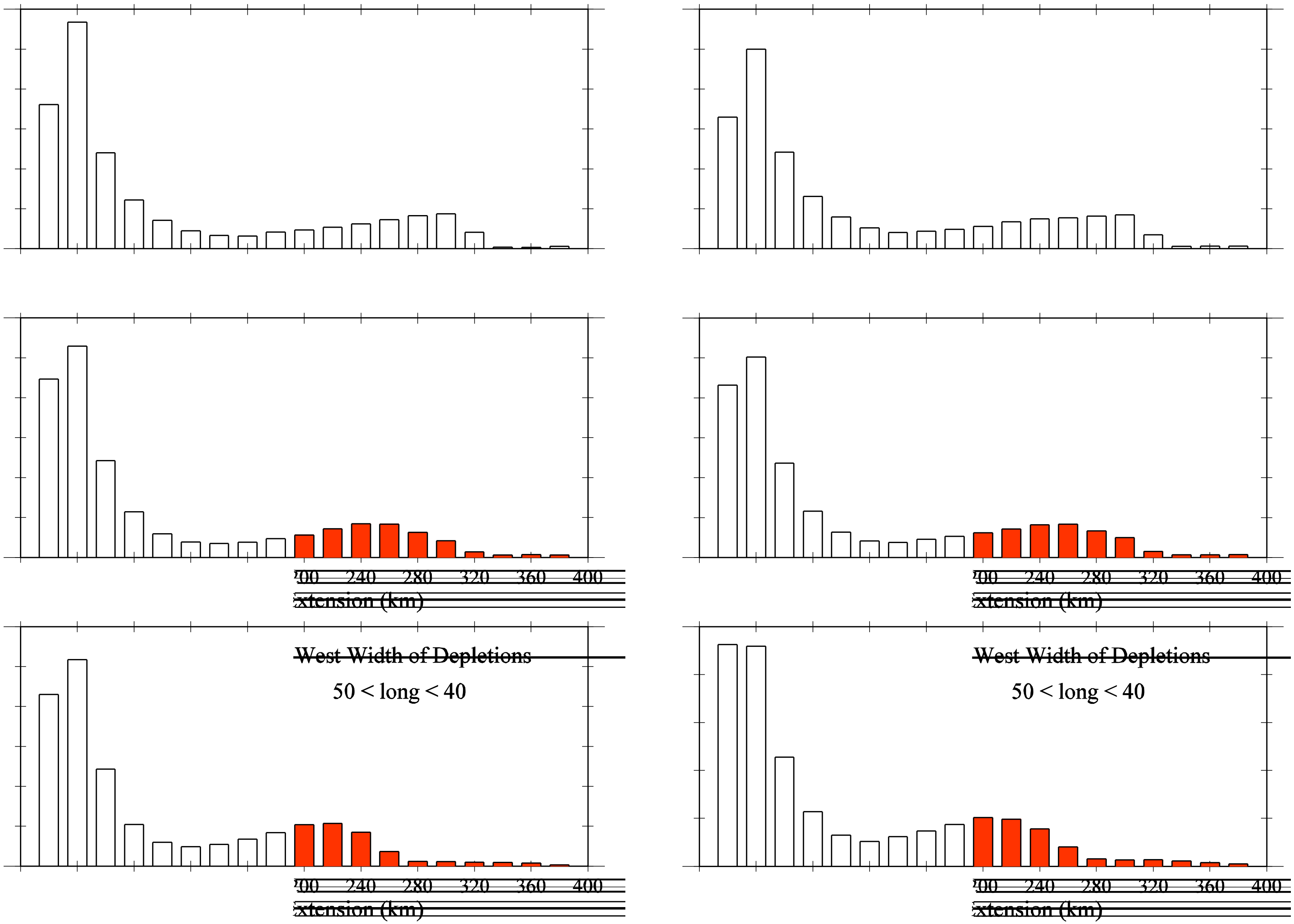

Conclusions

- **Work needs to be done to determine the triggering mechanism of plasma bubbles (gravity waves vs. other plasma instability process).**

- **LISN is a distributed observatory to study some aspects of space weather (plasma bubbles, ESF). It provides regional coverage of the day-to-day variability of the ionosphere over South America.**

Gravity Wave Seeding

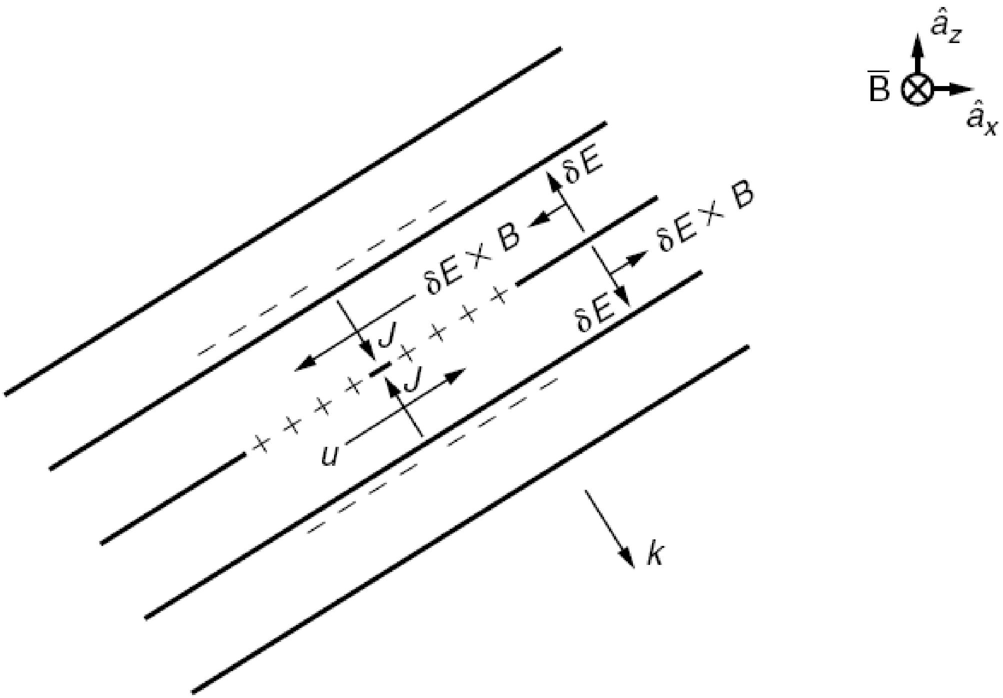

This diagram shows how the perturbation winds in a gravity wave generate electric fields.

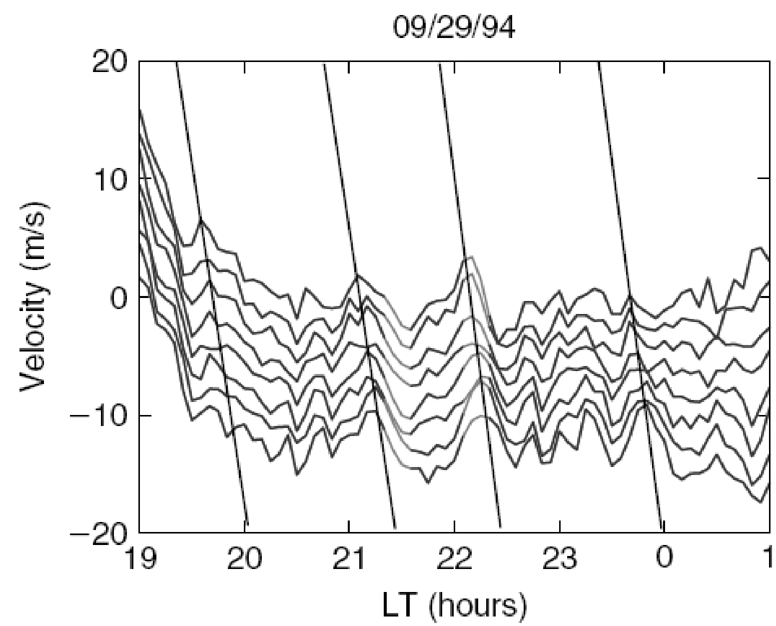

Vertical drift velocity measured at Jicamarca. The slanted lines have been aligned with peaks in the data to illustrate the downward phase velocity (Varney et al., 2009)

Shear effects on vortex fragmentation and ESF initiation

Radar imaging of the bottomside ESF at Jicamarca

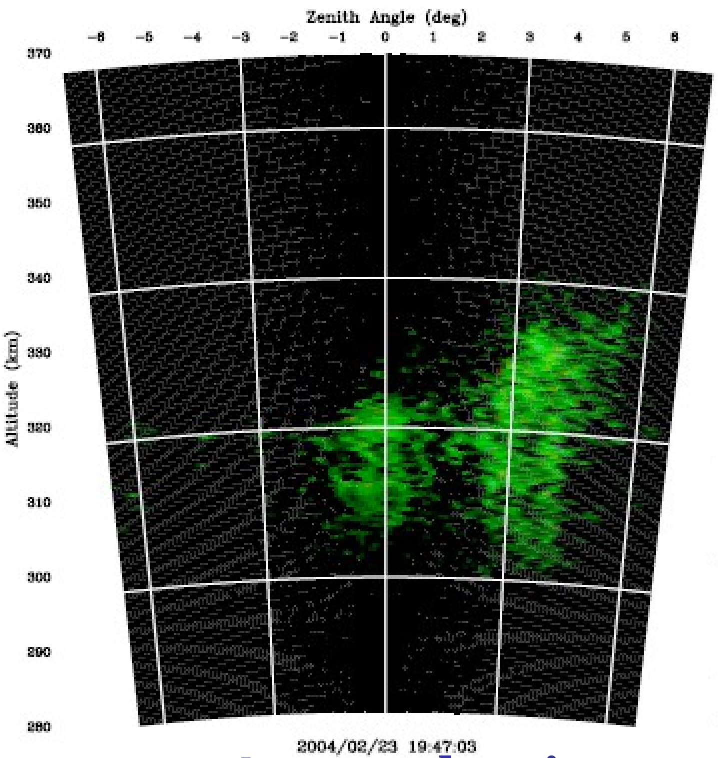

A snapshot in longitude and height

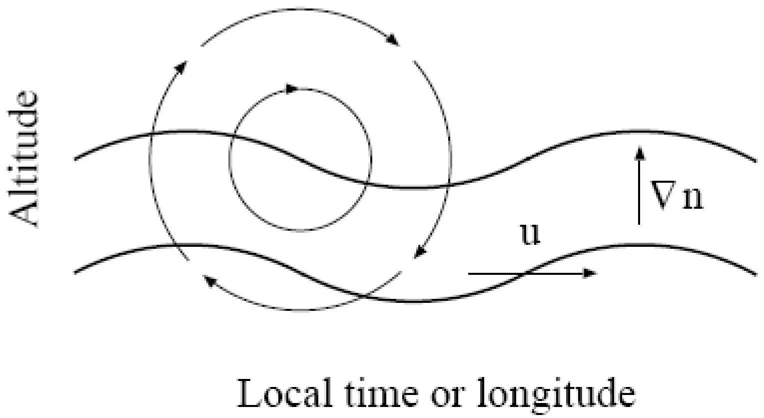

Locations where the horizontal wind is large in the plasma rest frame and antiparallel to to a component of the density gradient are unstable.

Hysell et al., Ann. Geophys., 2004.

GPS Scintillations observed east of 74°W

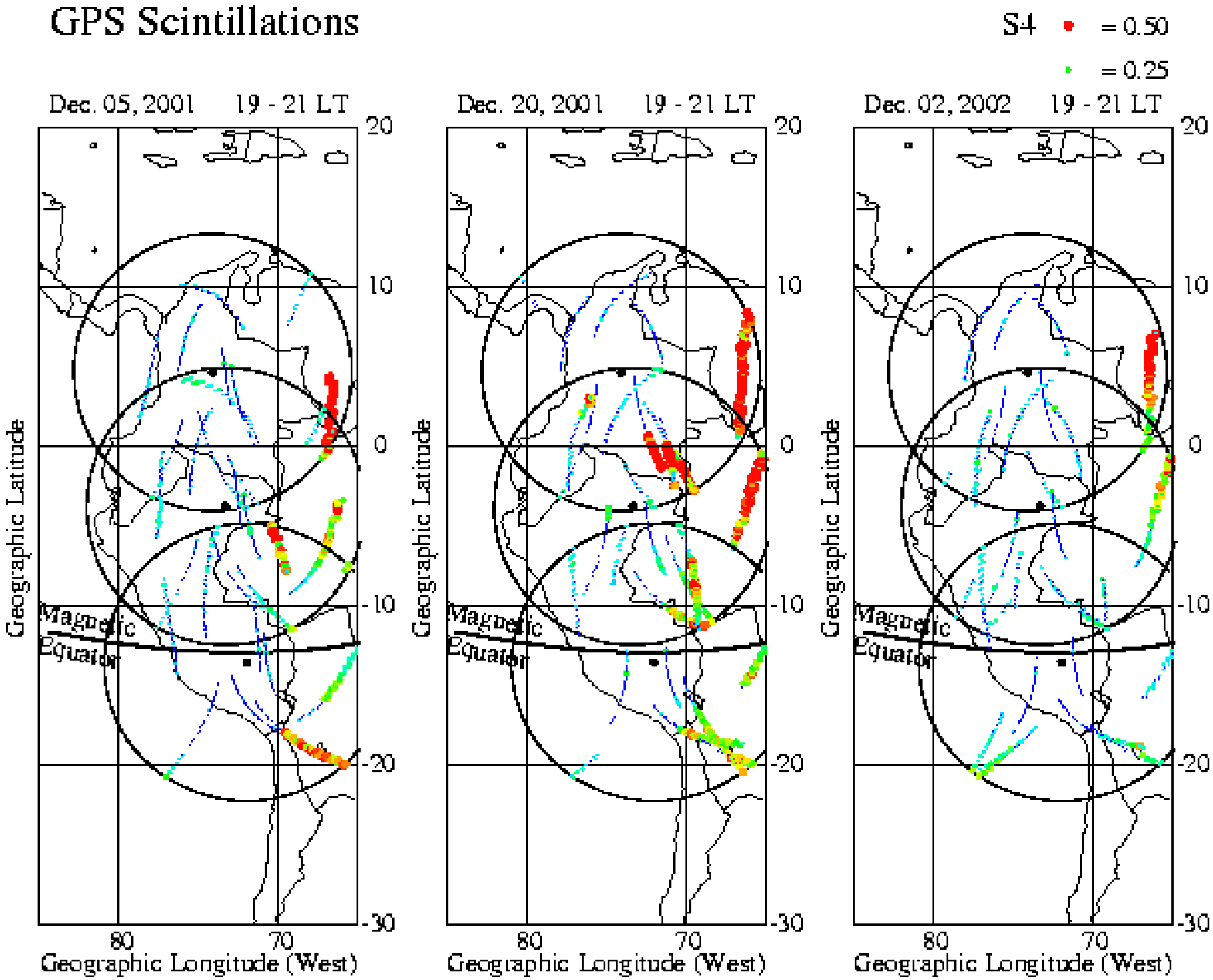

Can the thermospheric wind suppress gravity waves in the west coast?